Quantized Precoding for Massive MU-MIMO

Sven Jacobsson, Giuseppe Durisi, Mikael Coldrey, Tom Goldstein, and Christoph Studer

Abstract

Massive multiuser (MU) multiple-input multiple-output (MIMO) is foreseen to be one of the key technologies in fifth-generation wireless communication systems. In this paper, we investigate the problem of downlink precoding for a narrowband massive MU-MIMO system with low-resolution digital-to-analog converters (DACs) at the base station (BS). We analyze the performance of linear precoders, such as maximal-ratio transmission and zero-forcing, subject to coarse quantization. Using Bussgang's theorem, we derive a closed-form approximation of the achievable rate of the coarsely quantized system. Our results reveal that the infinite-resolution performance can be approached with DACs using only 3 to 4 bits of resolution, depending on the number of BS antennas and the number of user equipments (UEs). For the case of 1-bit DACs, we also propose novel nonlinear precoding algorithms that significantly outperform linear precoders at the cost of an increased computational complexity. Specifically, we show that nonlinear precoding incurs only a 3 dB penalty compared to the infinite-resolution case for an uncoded bit error rate of 10^{-3} in a system with 128 BS antennas that uses 1-bit DACs and serves 16 single-antenna UEs; in contrast, the penalty is about 8 dB for linear precoders.

Index Terms

Massive multi-user multiple-input multiple-output, digital-to-analog converter, Bussgang's theorem, minimum mean-square error precoding, convex optimization, semidefinite relaxation, Douglas-Rachford splitting, sphere precoding.

S. Jacobsson is with Ericsson Research and Chalmers University of Technology, Gothenburg, Sweden (e-mail: sven.jacobsson@ericsson.com).

G. Durisi is with Chalmers University of Technology, Gothenburg, Sweden (e-mail: durisi@chalmers.se).

M. Coldrey is with Ericsson Research, Gothenburg, Sweden (e-mail: mikael.coldrey@ericsson.com)

T. Goldstein is with the Department of Computer Science, University of Maryland, College Park, MD (e-mail: tomg@cs.umd.edu).

C. Studer is with the School of Electrical and Computer Engineering, Cornell University, Ithaca, NY (e-mail: studer@cornell.edu).

The work of S. Jacobsson and G. Durisi was supported by the Swedish Foundation for Strategic Research under grants SM13-0028 and ID14-0022, and by the Swedish Governmental Agency for Innovation Systems (VINNOVA) within the VINN Excellence center Chase.

The work of T. Goldstein was supported in part by the US National Science Foundation (NSF) under grant CCF-1535902 and by the US Office of Naval Research under grant N00014-15-1-2676.

The work of C. Studer was supported in part by Xilinx Inc. and by the US NSF under grants ECCS-1408006 and CCF-1535897.

The system simulator for quantized precoding will be made available on GitHub upon (possible) acceptance of the paper.

I. INTRODUCTION

Massive multiuser (MU) multiple-input multiple-output (MIMO) wireless systems, where the base station (BS) is equipped with several hundreds of antenna elements, promises significant improvements in spectral efficiency, energy efficiency, reliability, and coverage compared to traditional cellular systems [1]–[3]. Increasing the number of radio frequency (RF) chains at the BS could, however, lead to significant increases in hardware complexity, system costs, and circuit power consumption. Therefore, practical massive MU-MIMO systems may require low-cost and power-efficient hardware components at the BS. In this paper, we consider the downlink of massive MU-MIMO system, where the BS is equipped with low-resolution digital-to-analog converters (DACs) and transmits data to multiple, independent user equipments (UEs) in the same time-frequency resource.

For the quantization-free case (infinite-resolution DACs), the capacity region of the MU downlink Gaussian channel has been characterized in [4]–[7]. When channel state information (CSI) is known noncausally at the BS, dirty-paper coding (DPC) [8] is known to achieve the sum-rate capacity [6]. Several precoding algorithms to approach the DPC performance have been proposed (see, e.g., [9]–[12]). Most of these precoding methods are, however, computationally demanding, and their complexity scales unfavorably with the number of BS antennas, preventing their use for massive MU-MIMO. Linear precoding, on the other hand, is an attractive low-complexity approach to massive MU-MIMO downlink precoding, which offers competitive performance to DPC for large antenna arrays [13], [14].

These results assume that the RF circuitry connected to each antenna port at the BS is ideal. The impact of RF hardware impairments at the transmit side has been investigated in, e.g., [15]–[18]. Some of these results indicate that massive MU-MIMO exhibits a certain degree of resilience against RF impairments. The crude aggregate models used for characterizing such hardware impairments, however, are unable to accurately capture the distortion caused by low-resolution DACs.

A. What are the Benefits of Quantized Massive MU-MIMO?

One of the dominant sources of power consumption in massive MU-MIMO systems are the data converters at the BS. In the downlink, the transmit baseband signal at each RF chain is generated by a pair of DACs. The power consumption of these DACs increases exponentially with the resolution (in bits) and linearly with the bandwidth [19], [20]. In traditional multi-antenna systems, each RF port is connected to a pair of high-resolution DACs (e.g., 10-bit or more). For massive MU-MIMO systems with hundred or even thousands of antenna elements, this would lead to prohibitively high power consumption due to the large number of required DACs. Hence, the DAC resolution must be limited to keep the power budget within tolerable levels. In addition, the use of low-resolution DACs enables one to reduce the linearity and noise requirements of the surrounding RF circuitry; this has the potential to further reduce the power consumption and costs of the RF circuits at the BS. Furthermore, an often overlooked issue in massive MU-MIMO is the vast amount of data that must be transmitted from the fronthaul link to the baseband-processing unit. To make matters worse, in many deployment scenarios, these two units are separated by a large distance. Hence, lowering the DAC resolution is a potential solution to mitigate the data-rate bottleneck of the fronthaul link.

B. Relevant Prior Art

1) Quantized Receivers: Several recent contributions have studied the use of low-resolution analog-to-digital converters (ADCs) for the massive MU-MIMO *uplink*. In particular, there has been a significant interest in the 1-bit ADC case. For frequency-flat channels, the performance of 1-bit ADCs followed by linear detectors was analyzed in, e.g., [21]–[23], where it was shown that large achievable sum rates are supported. Similar conclusions were made in [24] for the frequency-selective case. Coarse quantization and nonlinear detection algorithms for frequency-selective channels were studied in [25], where it was found that 4 to 6 bits are sufficient to close the gap to the infinite-resolution case.

2) Low-PAR and Constant-Envelope Precoding: Hardware-aware precoding has previously been considered for massive MU-MIMO, with the goal of reducing the linearity requirements at the BS. In [26], the problem of joint MU precoding and peak-to-average power ratio (PAR) reduction was achieved by solving a convex optimization problem. Constant-envelope precoding was studied in [27], [28], which minimizes the PAR by transmitting constant-modulus signals only.

3) Quantized Precoding: In contrast to the uplink case, there has only been a small number of contributions that consider the massive MU-MIMO *downlink* with low-resolution DACs at the BS. In [29], the authors designed a linear-quantized precoder based on the minimum mean-square error (MMSE) criterion, taking into account the distortion caused by the DACs. For DACs with 4 to 6 bits resolution, the precoder proposed in [29] is shown to outperform conventional linear-quantized precoders for small-to-moderate-sized MIMO systems at high signal-to-noise ratio (SNR). Massive MU-MIMO systems with 1-bit DACs are investigated in [30], where it is shown that maximal ratio transmission (MRT) precoding results in manageable distortion levels. Still for the case of 1-bit DACs, zero-forcing (ZF) precoding for a Rayleigh-fading channel is considered in [31]. Interestingly, the authors show that the received signal can be made proportional to the transmitted signal when the number of BS antennas tend to infinity. This shows that the severe per-antenna distortion caused by the 1-bit DACs averages out over the antenna array. A linear precoder where the 1-bit quantized outcomes are rescaled in the analog domain was presented in [32]. There, the authors use the gradient projection algorithm to find a precoder that yields improved performance over the one reported in [29].

C. Contributions

We consider quantized precoding for the massive MU-MIMO downlink in frequency-flat channels. In contrast to [30]–[32], we do not restrict ourselves to 1-bit DACs and linear precoding. Specifically, we consider both *linear-quantized precoders*, where a linear precoder is followed by a finite-resolution DAC, and *nonlinear precoders*, where the data vector together with the CSI is used to directly generate the DAC outputs. Our contributions can be summarized as follows.

- We formulate the MMSE-optimal linear-quantized precoding problem and present low complexity, suboptimal linear-quantized precoders that yield approximate solutions to this problem. We use Bussgang's theorem to develop simple closed-form approximations for the rate achievable with linear-quantized precoding and low-resolution DACs. Through numerical simulations, we validate the accuracy of these approximations, and we show that only a small number of quantization bits are sufficient to close the performance gap to the infinite-resolution case. For the special case of 1-bit DACs, we develop a sharp lower bound on the achievable rate with linear precoding.
- For the 1-bit case, we develop a variety of low-complexity nonlinear precoders that achieve near-optimal performance. We show that the MMSE-optimal downlink precoding problem can be relaxed to a convex problem that can be solved in a computationally-efficient manner. We propose computationally efficient algorithms based on semidefinite relaxation, squared-ℓ_∞ norm relaxation, and sphere decoding, and we discuss advantages and limitations of each of these methods. Through numerical simulations, we demonstrate the superiority of nonlinear precoding over linear-quantized precoding.
- We investigate the sensitivity of the proposed precoders to channel-estimation errors and demonstrate that the proposed precoders are robust to imperfect CSI at the BS.

Our results reveal that massive MU-MIMO enables the use of low-resolution DACs at the BS without a significant performance loss in terms of error-rate performance and information-theoretic rates.

D. Notation

Lowercase and uppercase boldface letters designate column vectors and matrices, respectively. For a matrix $\mathbf{A}$, we denote its complex conjugate, transpose, and Hermitian transpose by $\mathbf{A}^*$, $\mathbf{A}^T$, and $\mathbf{A}^H$, respectively. The entry on the kth row and on the ℓth column is $[\mathbf{A}]_{k,\ell}$. For a vector $\mathbf{a}$, the kth entry is $[\mathbf{a}]_k$. We use $\mathbf{A} \succeq \mathbf{0}$ to indicate that the matrix $\mathbf{A}$ is positive semidefinite. The trace and the main diagonal of $\mathbf{A}$ are $\mathrm{tr}(\mathbf{A})$ and $\mathrm{diag}(\mathbf{A})$, respectively. The $M \times M$ identity and the all-zeros matrix are

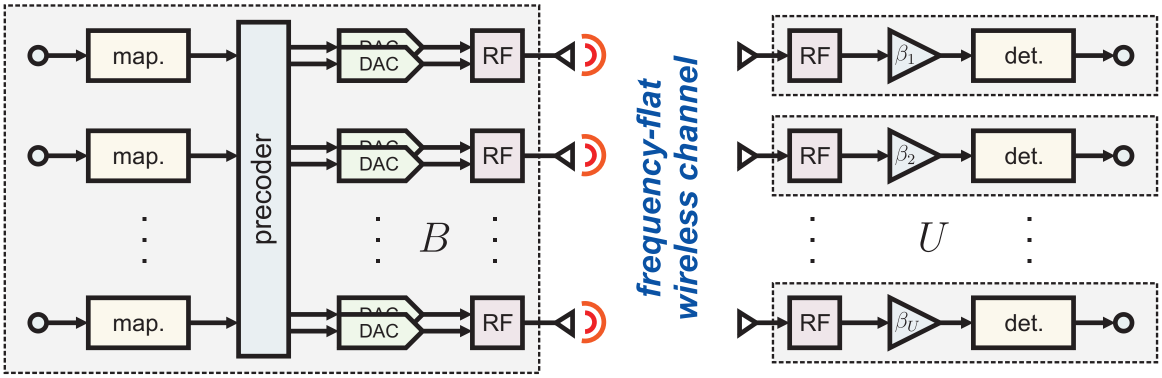

Fig. 1. Overview of the proposed quantized massive MU-MIMO downlink system. Left: B antenna massive MU-MIMO BS that performs quantized precoding to enable the use of low-resolution DACs; Right: U single-antenna UEs.

denoted by $\mathbf{I}_M$ and $\mathbf{0}_{M\times N}$, respectively. The real and imaginary parts of a complex vector $\mathbf{a}$ are $\Re\{\mathbf{a}\}$ and $\Im\{\mathbf{a}\}$, respectively. We use $\|\mathbf{a}\|_2$ and $\|\mathbf{a}\|_\infty$ to denote the ℓ_2-norm and the ℓ_∞-norm of $\mathbf{a}$, respectively. We use $\text{sgn}(\cdot)$ to denote the signum function, which is applied entry-wise to a vector and defined as $\text{sgn}(a) = +1$ for $a \geq 0$ and $\text{sgn}(a) = -1$ for $a < 0$. We further use $\mathbb{1}_\mathcal{A}(a)$ to denote the indicator function, which is defined as $\mathbb{1}_\mathcal{A}(a) = 1$ for $a \in \mathcal{A}$ and $\mathbb{1}_\mathcal{A}(a) = 0$ for $a \notin \mathcal{A}$. The multivariate complex-valued circularly-symmetric Gaussian probability density function (PDF) with covariance matrix $\mathbf{K}$ is denoted by $\mathcal{CN}(\mathbf{0}, \mathbf{K})$. We use $f(\cdot)$ to denote PDFs and $\mathbb{E}_\mathbf{x}[\cdot]$ to denote expectation in the random vector $\mathbf{x}$. The mutual information between two random vectors $\mathbf{x}$ and $\mathbf{y}$ is written as $\mathcal{I}(\mathbf{x};\mathbf{y})$.

E. Paper Outline

The rest of the paper is organized as follows. Section II introduces the system model and formulates the MMSE-optimal quantized precoding problem. Section III investigates linear-quantized precoders for massive MU-MIMO systems. Section IV deals with nonlinear precoding algorithms for the case of 1-bit DACs. Section V provides numerical simulation results and analyzes the robustness of the developed algorithms to channel-estimation errors. We conclude the paper in Section VI.

II. System Model and Quantized Precoding

A. System Model

We consider the downlink of a single-cell massive MU-MIMO system as illustrated in Fig. 1. The system consists of a BS with B antennas that serves U single-antenna UEs simultaneously and in the same time-frequency resource. The input-output relation of the downlink channel is modeled as

$$\mathbf{y} = \mathbf{H}\mathbf{x} + \mathbf{n}. \tag{1}$$

Here, the vector $\mathbf{y} = [y_1, \ldots, y_U]^T$ contains the received signals at all users, where $y_u \in \mathbb{C}$ is the signal received at the uth UE. The matrix $\mathbf{H} \in \mathbb{C}^{U \times B}$ models the downlink channel, and it is assumed to be perfectly known to the BS.[1] We shall also assume that the entries of $\mathbf{H}$ are independent circularly-symmetric complex Gaussian random variables with unit variance, i.e., $h_{u,b} = [\mathbf{H}]_{u,b} \sim \mathcal{CN}(0,1)$, for $u = 1, \ldots, U$, and $b = 1, \ldots, B$. The vector $\mathbf{n} \in \mathbb{C}^U$ in (1) models additive noise. We assume the noise to be i.i.d. circularly-symmetric complex Gaussian with variance N_0 per complex entry, i.e., $n_u \sim \mathcal{CN}(0, N_0)$, for $u = 1, \ldots, U$. We shall also assume that the noise level is known perfectly at the BS.[2]

The precoded vector is denoted by $\mathbf{x} \in \mathcal{X}^B$, where $\mathcal{X}$ represents the transmit alphabet; this set coincides with the set $\mathbb{C}$ of complex numbers in the case of infinite-resolution DACs. In real-world BS architectures with finite-resolution DACs, the set $\mathcal{X}$ is, however, a finite-cardinality alphabet. Specifically, we denote the set of possible real-valued DAC outputs (quantization labels) as $\mathcal{L} = \{\ell_0, \ldots, \ell_{L-1}\}$. We refer to $L = |\mathcal{L}|$ and $Q = \log_2 L$ as the number of quantization levels and the number of quantization bits per real dimension, respectively. For each BS antenna, we assume the same quantization alphabet for the real and the imaginary parts. Hence, the set of complex-valued DAC outputs at each antenna is $\mathcal{X} = \mathcal{L} \times \mathcal{L}$. Under these assumptions, the bth entry of the precoded vector $\mathbf{x}$ is $x_b = \ell_R + j\ell_I$ where $\ell_R, \ell_I \in \mathcal{L}$.

B. Precoding

The goal of precoding is to transmit constellation points $s_u \in \mathcal{O}$ for $u = 1, \ldots, U$ to each UE u, where $\mathcal{O}$ is the set of constellation points (e.g., QPSK). The BS uses the available CSI, namely the noncausal knowledge of the realization of the channel matrix $\mathbf{H}$, to precode the symbol vector $\mathbf{s} = [s_1, \ldots, s_U]^T$ into a B-dimensional precoded vector $\mathbf{x} = \mathcal{P}(\mathbf{s}, \mathbf{H})$. Here, the function $\mathcal{P}(\cdot,\cdot) : \mathcal{O}^U \times \mathbb{C}^{U \times B} \to \mathcal{X}^B$ represents the precoder. The precoded vector $\mathbf{x}$ must satisfy the average power constraint

$$\mathbb{E}_{\mathbf{s}}\left[\|\mathbf{x}\|_2^2\right] \leq P. \tag{2}$$

We define $\rho = P/N_0$ as the SNR.

Coherent transmission of data using multiple BS antennas leads to a *array gain*, which depends on the realization of the fading channel. We shall assume that the uth UE is able to rescale the received signal y_u by a factor $\beta_u \in \mathbb{R}$ to compute an estimate $\hat{s}_u \in \mathbb{C}$ of the transmitted symbol $s_u \in \mathcal{O}$ as follows:

$$\hat{s}_u = \beta_u y_u. \tag{3}$$

[1] In Section V-B, we will relax this assumption by investigating the impact of imperfect CSI to the robustness of the proposed quantized precoding algorithms.

[2] Knowledge of N_0 at the BS can be obtained by explicit feedback from the UEs to the BS.

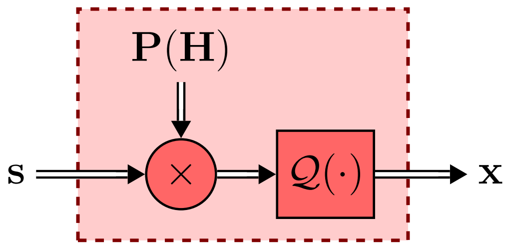

(a) Linear-quantized precoders: the precoder uses $\mathbf{H}$ to design a precoding matrix $\mathbf{P}$. The transmit vector is the quantized version of $\mathbf{Ps}$, i.e., $\mathbf{x} = \mathcal{Q}(\mathbf{Ps})$. Here, $\mathcal{Q}(\cdot)$ denotes the quantizers.

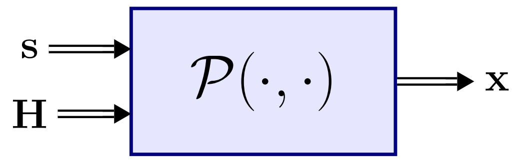

(b) Nonlinear precoders: the precoder uses $\mathbf{H}$ to directly compute the quantized transmit vector $\mathbf{x} \in \mathcal{X}^B$ as a nonlinear function of $\mathbf{s}$ and $\mathbf{H}$, i.e., $\mathbf{x} = \mathcal{P}(\mathbf{s}, \mathbf{H})$.

Fig. 2. Illustration of linear-quantized (a) and nonlinear (b) precoders.

The problem of downlink precoding has been studied extensively in the literature. Broadly speaking, the goal is to increase the signal power to the intended UEs while simultaneously reducing MU interference (MUI) [33]. There exist multiple formulations of this optimization problem based on different performance metrics (sum-rate throughput, worst-case throughput, error probability, etc.). We refer the interested reader to the tutorial [34] for a comprehensive overview.

Our goal is to design a precoder that minimizes the MSE between the estimated symbol vector $\hat{\mathbf{s}} = [\hat{s}_1, \ldots, \hat{s}_U]^T$ and the transmitted symbol vector $\mathbf{s}$ under the power constraint (2). This problem has been studied extensively for the case of infinite-resolution DACs (see, e.g., [35]–[37]).

If the BS is equipped with finite-resolution DACs, then the UEs will experience additional distortion compared to the infinite-resolution case, due to finite cardinality of the set $\mathcal{X}^B$ of possible precoder outputs. This implies that finding the MMSE-optimal precoder for BS architectures with finite-resolution DACs is a formidable task. In what follows, we present novel algorithms that efficiently compute approximate solutions to the quantized precoding problem. More specifically, we investigate two fundamentally distinct approaches: *linear-quantized precoding* (in Section III) and *nonlinear-quantized precoding* for the special case of 1-bit DACs (in Section IV). As illustrated in Fig. 2, linear-quantized precoders first perform linear processing (matrix-vector multiplication) followed by quantization; in contrast, nonlinear precoders use the transmit vector $\mathbf{s}$ together with the available CSI in order to directly compute the precoded vector $\mathbf{x}$. As it will be shown in Section V, nonlinear precoders outperform (often significantly) linear-quantized precoders in terms of error-rate performance at the cost of higher computational complexity.

III. Linear–Quantized Precoders

In the infinite-resolution case, linear precoders multiply the U-dimensional symbol vector $\mathbf{s}$ with a precoding matrix $\mathbf{P} \in \mathbb{C}^{B \times U}$ so that $\mathbf{x} = \mathbf{Ps}$. This approach is particularly attractive for massive

MU-MIMO systems due to (i) the relatively low computational complexity and (ii) the fact that even the simplest linear precoder, namely the MRT precoder, achieves virtually optimal performance in the large-antenna limit; see, e.g., [1]. Linear-quantized precoders inherit the first of these two advantages. Indeed, quantizing the precoded vector implies no additional computational complexity. For linear-quantized precoders, the precoded vector $\mathbf{x} \in \mathcal{X}^B$ is given by

$$\mathbf{x} = \mathcal{Q}(\mathbf{P}\mathbf{s}). \tag{4}$$

Here, $\mathcal{Q}(\cdot) : \mathbb{C}^B \to \mathcal{X}^B$ denotes the *quantizer-mapping* function, which is a nonlinear function that describes the joint operation of the $2B$ DACs at the BS.

The remainder of this section is organized as follows. We start by formulating the MMSE quantized precoding problem for linear-quantized precoders. We then describe the operation of the DACs and define the quantizer-mapping function. We then use Bussgang's theorem [38] to derive a lower bound on the sum-rate capacity for the case of 1-bit DACs at the BS. Finally, we derive a simple closed-form approximation of the rate achievable with Gaussian inputs for the more general case of Q-bit DACs.

A. The Linear-Quantized Precoding Problem

By restricting ourselves to linear-quantized precoding (LQP), the MMSE quantized precoding problem can be formulated as follows:

$$\text{(LQP)} \quad \begin{cases} \underset{\mathbf{P}\in\mathbb{C}^{B\times U},\, \beta\in\mathbb{R}}{\text{minimize}} & \mathbb{E}_{\mathbf{s}}\Big[\|\mathbf{s} - \beta\mathbf{H}\mathcal{Q}(\mathbf{P}\mathbf{s})\|_2^2\Big] + \beta^2 U N_0 \\ \text{subject to} & \mathbb{E}_{\mathbf{s}}\Big[\|\mathbf{x}\|_2^2\Big] \leq P \text{ and } \beta > 0. \end{cases} \tag{5}$$

The resulting precoding matrix $\mathbf{P}^{\text{LQP}}$ and the associated scalar β^{LQP} are referred to as the optimal solution to the problem (LQP). Here, we have introduced the parameter $\beta \in \mathbb{R}$ to account for the array gain. In (LQP), we have restricted ourselves to the case in which the precoder results in the same gain $\beta \in \mathbb{R}$ for all UEs. For this case, the per-channel MSE between the transmitted symbols $\mathbf{s}$ and the estimated symbols $\hat{\mathbf{s}} = \beta\mathbf{y}$ can be written as

$$\mathbb{E}_{\mathbf{s}}\Big[\|\hat{\mathbf{s}} - \mathbf{s}\|_2^2\Big] = \mathbb{E}_{\mathbf{s}}\Big[\|\mathbf{s} - \beta\mathbf{H}\mathbf{x}\|_2^2\Big] + \beta^2 U N_0. \tag{6}$$

By replacing $\mathbf{x} = \mathcal{Q}(\mathbf{P}\mathbf{s})$, we recognize (6) as the objective function in (5). Note that the array gain the precoder attempts to achieve may differ from the actual array gain experienced by the uth UE. Therefore, we let each UE scale the received signal by an individual factor β_u, for $u = 1, \ldots, U$ (see Fig. 1).

Solving (5) in closed form is a challenging task due to the nonlinear operation of the DACs, captured by the quantizer-mapping function $\mathcal{Q}(\cdot)$. An approximate solution to (5) was presented in [29]. This solution is obtained by approximating the statistics of the distortion caused by the DACs. We shall consider a different approach. Specifically, we design linear precoders that assume infinite-resolution DACs at the BS, and then quantize the resulting precoded vector. Such linear-quantized precoders have the advantage that the precoding matrix $\mathbf{P}$ does not depend on the resolution of the DACs. Furthermore, as we shall see in Section V-A, the difference in error-rate performance between the precoders found using our approach and the precoder presented in [29] is negligible. We next review a variety of linear precoding algorithms.

1) WF precoding: For the case when the BS is equipped with infinite-resolution DACs, the solution to (5) is the Wiener filter (WF) precoder [36]:

$$\mathbf{P}^{\text{WF}} = \frac{1}{\beta^{\text{WF}}}\mathbf{H}^H(\mathbf{H}\mathbf{H}^H + UN_0\mathbf{I}_U)^{-1} \tag{7}$$

where

$$\beta^{\text{WF}} = \sqrt{\frac{1}{P}\,\text{tr}((\mathbf{H}\mathbf{H}^H + UN_0\mathbf{I}_U)^{-1}\mathbf{H}\mathbf{H}^H(\mathbf{H}\mathbf{H}^H + UN_0\mathbf{I}_U)^{-1})}. \tag{8}$$

We write the resulting precoded vector as $\mathbf{x}^{\text{WF}} = \mathcal{Q}\big(\mathbf{P}^{\text{WF}}\mathbf{s}\big)$.

2) ZF precoding: With ZF precoding, the BS nulls the multiuser interference by choosing as precoding matrix the pseudo-inverse of the channel matrix. The ZF precoding matrix is obtained from (7) by setting the noise variance N_0 to zero, which yields $\mathbf{P}^{\text{ZF}} = \frac{1}{\beta^{\text{ZF}}}\mathbf{H}^\dagger$, where $\mathbf{H}^\dagger = \mathbf{H}^H(\mathbf{H}\mathbf{H}^H)^{-1}$ is the pseudo-inverse of the channel matrix $\mathbf{H}$, and $\beta^{\text{ZF}} = \sqrt{\frac{1}{P}\,\text{tr}((\mathbf{H}\mathbf{H}^H)^{-1})}$. The resulting precoded vector is $\mathbf{x}^{\text{ZF}} = \mathcal{Q}\big(\mathbf{P}^{\text{ZF}}\mathbf{s}\big)$.

3) MRT precoding: The MRT precoder maximizes the power directed towards each UE, ignoring MUI. The precoding matrix can be obtained from (7) by letting the noise variance N_0 tend to infinity, which yields $\mathbf{P}^{\text{MRT}} = \frac{1}{\beta^{\text{MRT}}B}\mathbf{H}^H$ and $\beta^{\text{MRT}} = \frac{1}{B}\sqrt{\frac{1}{P}\,\text{tr}(\mathbf{H}\mathbf{H}^H)}$. The resulting precoded vector is $\mathbf{x}^{\text{MRT}} = \mathcal{Q}\big(\mathbf{P}^{\text{MRT}}\mathbf{s}\big)$.

B. Uniform Quantization of a Complex-Valued Vector

We shall model the DACs as symmetric uniform quantizers with step size Δ. When a signal is quantized, the average power in the signal is in general not preserved. Therefore, we further assume that the output of the quantizer is scaled by a constant $\alpha \in \mathbb{R}$, to ensure that the transmit power constraint (2) remains to be satisfied. We start by defining a set of quantization labels $\mathcal{L} = \{\ell_0, \ldots, \ell_L\}$ with entries

$$\ell_i = \alpha\Delta\left(i - \frac{L-1}{2}\right), \quad i = 0, \ldots, L-1. \tag{9}$$

Furthermore, let $\mathcal{T} = \{\tau_0, \ldots, \tau_L\}$, where $-\infty = \tau_0 < \tau_1 < \cdots < \tau_{L-1} < \tau_L = \infty$ specify the set of $L+1$ quantization thresholds. For uniform quantizers, the quantization thresholds are given by

$$\tau_i = \Delta\left(i - \frac{L}{2}\right), \quad i = 1, \ldots, L-1. \tag{10}$$

The quantizer-mapping function $\mathcal{Q}(\cdot)$ can uniquely be described by the set of quantization labels $\mathcal{L}$ and the set of quantization thresholds $\mathcal{T}$. The DACs map $\mathbf{z} \in \mathbb{C}$ with entries $\{z_b\}$ into the quantized output $\mathbf{x}$ with entries $\{x_b\}$ in the following way: if $\Re\{z_b\} \in [\tau_k, \tau_{k+1})$ and $\Im\{z_b\} \in [\tau_l, \tau_{l+1})$, then $x_b = \ell_k + j\ell_l$.

The step size Δ of the quantizers should be chosen to minimize the distortion between the quantized and nonquantized vector. Unfortunately, the optimal step size Δ depends on the distribution of the input [39], which in our case depends on the precoder and on the signaling scheme. We therefore simply set the labels and thresholds so as they minimize the distortion under the assumption that the per-antenna input to the quantizers is $\mathcal{CN}(0, P/B)$-distributed. The optimal step size can then be found numerically (see e.g., [40] for details).

In the extreme case of 1-bit DACs, the quantizer-mapping function reduces to

$$\mathcal{Q}(\mathbf{z}) = \sqrt{\frac{P}{2B}}\big(\mathrm{sgn}(\Re\{\mathbf{z}\}) + j\,\mathrm{sgn}(\Im\{\mathbf{z}\})\big). \tag{11}$$

Here, we have chosen the set of possible complex-valued quantization outcomes per antenna to be $\mathcal{X} = \{\sqrt{P/(2B)}\,(\pm 1 \pm j)\}$, which ensures that the power constraint in (2) is satisfied with equality.

C. Signal Decomposition using Bussgang's Theorem

Quantizing the precoded signal causes a distortion $\mathcal{Q}(\mathbf{Ps}) - \mathbf{Ps}$ that is correlated with the input of the quantizer. However, for Gaussian inputs, Bussgang's theorem [38] allows us to decompose the quantized signal into linear function of the input to the quantizers and a distortion term that is *uncorrelated* with the input to the quantizers [41]. This will allow us to characterize the achievable rates with Gaussian inputs. We start by stating Bussgang's theorem [38], [41].

Theorem 1: Consider two zero-mean jointly complex Gaussian random variables x and y. Assume that x is passed through a nonlinear function $g(\cdot) : \mathbb{C} \to \mathbb{C}$ that acts independently on the real and imaginary components of x. Then, the covariance between $g(x)$ and y is given by

$$\mathbb{E}[g(x)y^*] = \frac{\mathbb{E}[g(x)x^*]}{\mathbb{E}[xx^*]}\,\mathbb{E}[xy^*]\,. \tag{12}$$

Bussgang's theorem has recently been used to analyze massive MU-MIMO uplink systems with 1-bit ADCs (see, e.g., [23], [24]). It was also used in [30] to approximate the resulting distortion levels caused by MRT precoding and 1-bit quantization in the massive MIMO downlink. We shall use Theorem 1 to characterize the performance of linear precoding subject to quantization with Q-bit uniform DACs. As a first step, we establish the following result, whose proof is given in Appendix A.

Theorem 2: Let $\mathbf{x} = \mathcal{Q}(\mathbf{P}\mathbf{s})$ denote the output from a set of uniform quantizers described by the quantizer-mapping function $\mathcal{Q} : \mathbb{C}^B \to \mathcal{X}^B$. Assume that $\mathbf{P} \in \mathbb{C}^{B\times U}$ and $\mathbf{s} \sim \mathcal{CN}(\mathbf{0}, \mathbf{I}_U)$. Then, the quantized vector $\mathbf{x}$ can be decomposed as

$$\mathbf{x} = \mathbf{G}\mathbf{P}\mathbf{s} + \mathbf{d}, \tag{13}$$

where the distortion $\mathbf{d}$ and the signal $\mathbf{s}$ are uncorrelated. Furthermore, $\mathbf{G} \in \mathbb{R}^{B\times B}$ is the following diagonal matrix:

$$\mathbf{G} = \frac{\alpha\Delta}{\sqrt{\pi}} \operatorname{diag}\!\left(\mathbf{P}\mathbf{P}^H\right)^{-1/2} \sum_{i=1}^{L-1} \exp\!\left(-\Delta^2\left(i - \frac{L}{2}\right)^2 \operatorname{diag}\!\left(\mathbf{P}\mathbf{P}^H\right)^{-1}\right). \tag{14}$$

Here, L and Δ denote the number of levels and the step size of the DACs, respectively.

The following corollary is a well-known result for the case of 1-bit quantization (see, e.g., [23], [24]). The proof follows from setting in (14) $L = 2$ and $\alpha\Delta = \sqrt{2P/B}$ to satisfy the power constraint in (2).

Corollary 3: For the case of 1-bit DACs, the matrix $\mathbf{G}$ in (14) reduces to

$$\mathbf{G} = \sqrt{\frac{2P}{\pi B}} \operatorname{diag}\!\left(\mathbf{P}\mathbf{P}^H\right)^{-1/2}. \tag{15}$$

Let now $\mathbf{h}_u^T$ denote the uth row of the channel matrix $\mathbf{H}$ and $\mathbf{p}_u$ the uth column of the precoding matrix $\mathbf{P}$. Using (13), we can express the received signal y_u at UE u as follows:

$$y_u = \mathbf{h}_u^T(\mathbf{G}\mathbf{P}\mathbf{s} + \mathbf{n}) = \mathbf{h}_u^T\mathbf{G}\mathbf{p}_u s_u + \underbrace{\textstyle\sum_{v\neq u} \mathbf{h}_u^T\mathbf{G}\mathbf{p}_v s_v + \mathbf{h}_u^T\mathbf{d}}_{=e_u} + \underbrace{\mathbf{h}_u^T\mathbf{n}}_{=\tilde{n}_u} = \mathbf{h}_u^T\mathbf{G}\mathbf{p}_u s_u + e_u + \tilde{n}_u. \tag{16}$$

Here, the error term e_u captures both the MUI and the distortion caused by the finite-resolution DACs. Note that e_u and s_u are uncorrelated. Indeed,

$$\mathbb{E}_{\mathbf{s}}[e_u s_u^*] = \textstyle\sum_{v\neq u} \mathbf{h}_u^T\mathbf{G}\mathbf{p}_v\, \mathbb{E}_{\mathbf{s}}[s_v s_u^*] + \mathbf{h}_u^T\, \mathbb{E}_{\mathbf{s}}[\mathbf{d}s_u^*] = 0. \tag{17}$$

We shall next use the decomposition in (16) to analyze the performance of linear-quantized precoders.

D. Achievable Rate Lower Bound for 1-bit DACs

We assume that each UE is able to scale its received signal y_u by $\beta_u = (\mathbf{h}_u^T \mathbf{G} \mathbf{p}_u)^{-1}$ to obtain the following estimate:

$$\hat{s}_u = \beta_u y_u = s_u + \beta_u (e_u + \tilde{n}_u). \tag{18}$$

Learning β_u requires each UE to be able to estimate accurately its channel gain. This is a reasonable assumption provided that the channel coherence interval is sufficiently long [42].

The nonlinear operation of the DACs prevents one to characterize the probability distribution of the error term e_u in closed form, which makes it difficult to compute the achievable rates. One can, however, lower-bound the achievable rate using the so called "auxiliary-channel lower bound" [43, p. 3503], which gives the rates achievable with a mismatched decoder (see [44, ch. 1] for a recent review on the subject). As auxiliary channel, we take the one with output

$$\tilde{s}_u = s_u + \beta_u (\tilde{e}_u + \tilde{n}_u), \tag{19}$$

where $\tilde{e}_u \sim \mathcal{CN}\big(0, \mathbb{E}_{\mathbf{s}}\big[|e_u|^2\big]\big)$ has the same variance as the actual error term e_u but is Gaussian distributed. This auxiliary channel is relevant for the case of *nearest-neighbor* decoding (also known as *minimum distance* decoding). Then, by standard manipulations of the mutual information, we can bound the achievable rate R_u for UE $u = 1, 2, \ldots, U$ as follows:

$$\begin{aligned} R_u &= \mathbb{E}_{\mathbf{H}}[\mathcal{I}(s_u; \hat{s}_u \,|\, \mathbf{H})] && (20)\\ &= \mathbb{E}_{s_u, \hat{s}_u, \mathbf{H}}\left[\log_2\!\left(\frac{f_{\hat{s}_u | s_u, \mathbf{H}}(\hat{s}_u | s_u, \mathbf{H})}{f_{\hat{s}_u \,|\, \mathbf{H}}(\hat{s}_u \,|\, \mathbf{H})}\right)\right] && (21)\\ &\geq \mathbb{E}_{s_u, \hat{s}_u, \mathbf{H}}\left[\log_2\!\left(\frac{f_{\tilde{s}_u | s_u, \mathbf{H}}(\hat{s}_u | s_u, \mathbf{H})}{f_{\tilde{s}_u \,|\, \mathbf{H}}(\hat{s}_u \,|\, \mathbf{H})}\right)\right] && (22)\\ &= \mathbb{E}_{\mathbf{H}}[\log_2(1 + \gamma_u)] && (23) \end{aligned}$$

where

$$\gamma_u = \frac{\left|\mathbf{h}_u^T \mathbf{G} \mathbf{p}_u\right|^2}{\sum_{v \neq u} \left|\mathbf{h}_u^T \mathbf{G} \mathbf{p}_v\right|^2 + \mathbf{h}_u^T \mathbf{C}_{\mathbf{dd}} \mathbf{h}_u^* + N_0} \tag{24}$$

is the signal-to-interference-noise-and-distortion ratio (SINDR) at the uth UE.[3] Here, $\mathbf{C}_{\mathbf{dd}} = \mathbb{E}_{\mathbf{s}}\big[\mathbf{d}\mathbf{d}^H\big]$ denotes the covariance of the distortion $\mathbf{d}$, which can be written as

$$\mathbf{C}_{\mathbf{dd}} = \mathbf{C}_{\mathbf{xx}} - \mathbf{G}\mathbf{P}\mathbf{P}^H\mathbf{G}^H \tag{25}$$

[3] One can establish (23) also by noting that Gaussian noise is the worst noise for Gaussian inputs [45].

where $\mathbf{C_{xx}} = \mathbb{E}_{\mathbf{s}}\left[\mathbf{x}\mathbf{x}^H\right]$ is the covariance of the quantized signal $\mathbf{x} = \mathcal{Q}(\mathbf{Ps})$. In the special case of 1-bit DACs, $\mathbf{C_{xx}}$ can be written in closed-form as [46], [47]

$$\mathbf{C_{xx}} = \frac{P}{\pi B}\Big(\sin^{-1}\Big(\operatorname{diag}(\mathbf{PP}^H)^{-\frac{1}{2}}\Re\{\mathbf{PP}^H\}\operatorname{diag}(\mathbf{PP}^H)^{-\frac{1}{2}}\Big) + j\sin^{-1}\Big(\operatorname{diag}(\mathbf{PP}^H)^{-\frac{1}{2}}\Im\{\mathbf{PP}^H\}\operatorname{diag}(\mathbf{PP}^H)^{-\frac{1}{2}}\Big)\Big). \tag{26}$$

Thus, using (25) and (26), the SINDR in (24) can be computed exactly for the case of 1-bit DACs. Substituting (24) in (23), one obtains a lower bound on the per-user achievable rate with Gaussian signaling for the 1-bit DAC case. Unfortunately, no closed-form expression for $\mathbf{C_{xx}}$ is available in the multi-bit DAC case. We address this problem in the next section.

E. Asymptotic Achievable Rate Approximation for Multi-Bit DACs

In this section, we provide for the multi-bit DAC case, an approximation of (24) derived under the assumption that both B and U are large, and relying on standard random matrix theory arguments. Specifically, let

$$G = \alpha\Delta\sqrt{\frac{B}{\pi P}}\sum_{i=1}^{L-1}\exp\left(-\frac{B\Delta^2}{P}\left(i-\frac{L}{2}\right)^2\right) \tag{27}$$

where

$$\alpha = \left(2B\Delta^2\left(\left(\frac{L-1}{2}\right)^2 - 2\sum_{i=1}^{L-1}\left(i-\frac{L}{2}\right)\Phi\left(\sqrt{2B\Delta^2}\left(i-\frac{L}{2}\right)\right)\right)\right)^{-1/2} \tag{28}$$

ensures that the power constraint (2) is satisfied. In (27), the function $\Phi(x) = \int_{-\infty}^{x}\frac{1}{\sqrt{2\pi}}e^{-t^2/2}\,dt$ is the cumulative distribution function of a Gaussian random variable. Let also $\bar{\rho}$ be defined as follows:

$$\bar{\rho} = \frac{G^2\rho}{(1-G^2)\rho+1}. \tag{29}$$

Following the same approach as in [48]–[50], one can show that, for the three linear-quantized precoders (WF, ZF, and MRT) introduced in Section III-A, the SINDR γ_u in (24) can be approximated for large B and U by

$$\bar{\gamma}^{\text{WF}} = \frac{\bar{\rho}}{2}\left(\frac{B}{U}-1\right) + \frac{1}{2}\sqrt{\bar{\rho}^2\left(\frac{B}{U}-1\right)^2 + 2\bar{\rho}\left(\frac{B}{U}+1\right)+1} - \frac{1}{2} \tag{30}$$

$$\bar{\gamma}^{\text{ZF}} = \bar{\rho}\left(\frac{B}{U}-1\right) \tag{31}$$

$$\bar{\gamma}^{\text{MRT}} = \frac{\bar{\rho}B}{\bar{\rho}(U-1)+U}. \tag{32}$$

Substituting (30)-(32) into (23), one gets a large B and U approximation of the achievable rate with Gaussian signaling and nearest-neighbor decoding. In Section V, we will verify through numerical simulations that this approximations is accurate already for realistic values of B and U.

IV. Nonlinear Precoders for 1-Bit DACs

We now investigate nonlinear precoders that seek approximate solutions to the MMSE-optimal problem detailed in Section II-B. We shall focus on the extreme case of 1-bit DACs, for which the problem simplifies and efficient numerical algorithms can be developed.

We start by noting that, in the 1-bit case, all DAC outcomes have equal amplitude, and that $\|\mathbf{x}\|_2^2 = P$ if one sets $\alpha\Delta = \sqrt{2P/B}$ in (9). This observation allows us to formulate the 1-bit quantized precoding (QP) problem as follows:

$$\text{(QP)} \quad \begin{cases} \underset{\mathbf{x}\in\mathcal{X}^B,\, \beta\in\mathbb{R}}{\text{minimize}} & \|\mathbf{s} - \beta\mathbf{H}\mathbf{x}\|_2^2 + \beta^2 U N_0 \\ \text{subject to} & \beta > 0. \end{cases} \tag{33}$$

Here, $\mathcal{X} = \left\{\sqrt{P/(2B)}\,(\pm 1 \pm j)\right\}$. The resulting precoded vector $\mathbf{x}^{\text{QP}}$ and the associated precoding factor β^{QP} are referred to as the optimal solution to the problem (33).

Compared to the problem (LQP) in (5), where we minimize the MSE averaged over the symbol vector $\mathbf{s}$ (for a given $\mathbf{H}$), in (QP) we minimize the MSE for every realization of the symbol vector $\mathbf{s}$. By solving the optimization problem on a per-symbol basis, the resulting β depends on the instantaneous value of the precoded vector $\mathbf{x}$, and, hence, on $\mathbf{s}$. This is in contrast to the linear-quantized case, where β is independent of the current symbol realization and depends only on $\mathbf{H}$.[4].

We note that (QP) in (33) resembles an ℓ_2-norm regularized closest-vector problem (CVP), with the unique feature that the discrete set of vectors is parametrized by the continuous precoding factor β. This prevents the straightforward use of conventional algorithms to approximate CVPs [51], [52]. Since the objective function in (33) is a quadratic function in β, we can compute the optimal value of β as

$$\hat{\beta}(\mathbf{x}) = \frac{\Re\{\mathbf{s}^H\mathbf{H}\mathbf{x}\}}{\mathbf{x}^H\left(\mathbf{H}^H\mathbf{H} + \frac{UN_0}{P}\mathbf{I}_B\right)\mathbf{x}} = \frac{\Re\{\mathbf{s}^H\mathbf{H}\mathbf{x}\}}{\|\mathbf{H}\mathbf{x}\|_2^2 + UN_0} \tag{34}$$

which depends on $\mathbf{x}$. Inserting (34) into the objective function in (33), we obtain the following equivalent formulation of the QP problem

$$\underset{\mathbf{x}\in\mathcal{X}^B}{\text{minimize}} \quad \left\|\mathbf{s} - \hat{\beta}(\mathbf{x})\mathbf{H}\mathbf{x}\right\|_2^2 + \hat{\beta}(\mathbf{x})^2 U N_0. \tag{35}$$

[4]We shall discuss the impact of the dependence of β on $\mathbf{s}$ on the receive-side processing in Section IV-D

In order to obtain β^{QP}, we can then simply evaluate (34) for the optimal vector $\mathbf{x}^{\text{QP}}$. We emphasize that a straightforward exhaustive search to solve (QP) requires the evaluation of $|\mathcal{X}|^B = 4^B$ candidate vectors, a quantity that grows exponentially with the number of BS antennas B. For a system with $B = 128$ antennas at the BS, this approach would require us to evaluate the objective function more than 10^{77} times (more than 10 quattuorvigintillions times). In fact, for a fixed value of β, the problem (QP) is a closest vector problem that is NP-hard [53]. This implies that there are no known algorithms to solve such problems efficiently for large values of B.[5] Hence, alternative algorithms that solve a lower complexity version of the QP problem are required for massive MU-MIMO systems.

In order to develop such computationally-efficient algorithms, we start by defining the auxiliary vector $\mathbf{b} = \beta\mathbf{x}$ and rewrite (33) in the following equivalent form

$$\underset{\mathbf{b}\in\mathcal{B}^B}{\text{minimize}} \quad \|\mathbf{s} - \mathbf{H}\mathbf{b}\|_2^2 + \frac{UN_0}{P}\|\mathbf{b}\|_2^2 \tag{36}$$

where $\mathcal{B} = \left\{\sqrt{P/(2B)}\,(\pm\beta \pm j\beta)\,,\ \text{for all}\ \beta > 0\right\}$. Here, we have used the fact that $\beta^2 = \|\mathbf{b}\|_2^2/P$. Let $\mathbf{b}^{\text{QP}}$ be the solution to (36). The resulting precoding vector is obtained by scaling each entry of $\mathbf{b}^{\text{QP}}$ so that it belongs to the set $\mathcal{X}$. Clearly, $1/\beta^{\text{QP}}$ is the scaling parameter.

It turns out convenient to transform the complex-valued problem (36) into an equivalent real-valued problem using the following standard definitions:

$$\mathbf{b}_{\mathbb{R}} = \begin{bmatrix} \Re\{\mathbf{b}\} \\ \Im\{\mathbf{b}\} \end{bmatrix},\ \mathbf{s}_{\mathbb{R}} = \begin{bmatrix} \Re\{\mathbf{s}\} \\ \Im\{\mathbf{s}\} \end{bmatrix},\ \text{and}\ \mathbf{H}_{\mathbb{R}} = \begin{bmatrix} \Re\{\mathbf{H}\} & -\Im\{\mathbf{H}\} \\ \Im\{\mathbf{H}\} & \Re\{\mathbf{H}\} \end{bmatrix}. \tag{37}$$

These definitions enable us to rewrite (36) as

$$\underset{\mathbf{b}_{\mathbb{R}}\in\mathcal{B}_{\mathbb{R}}^{2B}}{\text{minimize}} \quad \|\mathbf{s}_{\mathbb{R}} - \mathbf{H}_{\mathbb{R}}\mathbf{b}_{\mathbb{R}}\|_2^2 + \frac{UN_0}{P}\|\mathbf{b}_{\mathbb{R}}\|_2^2 \tag{38}$$

where $\mathcal{B}_{\mathbb{R}} = \left\{\pm\sqrt{P/(2B)}\,\beta,\ \text{for all}\ \beta > 0\right\}$ is the set of scaled antipodal outcomes per 1-bit DAC. We shall next develop a variety of nonlinear precoding methods that find approximate solutions to the problem (38).

A. Semidefinite Relaxation

Semidefinite relaxation (SDR) is a well-established technique to develop approximate algorithms for a variety of discrete programming problems [54]. For example, SDR is commonly used to find near-ML

[5] As we will show in Section IV-C, we can—in some cases—design branch-and-bound methods (such as sphere-decoding methods) that allow us to solve the quantized precoding problem efficiently for moderately-sized problems. For massive MU-MIMO systems with hundreds of antennas, however, such methods still exhibit prohibitive computational complexity.

solutions for the MU-MIMO detection problem (see, e.g., [54], [55]). For the case when the BS is equipped with infinite-resolution DACs, SDR has been used for downlink precoding in [56], [57]. We next show how SDR can be used to find approximate solutions to (33).

In our context, SDR involves relaxing (38) to a semidefinite program (SDP) as follows. We start by writing the real-valued problem (38) in the following equivalent form [54]:

$$\begin{aligned} \underset{\mathbf{b}_{\mathbb{R}}\in\mathbb{R}^{2B},\, \psi\in\{\pm1\}}{\text{minimize}} \quad & \|\psi\mathbf{s}_{\mathbb{R}} - \mathbf{H}_{\mathbb{R}}\mathbf{b}_{\mathbb{R}}\|_2^2 + \frac{UN_0}{P}\|\mathbf{b}_{\mathbb{R}}\|_2^2 \\ \text{subject to} \quad & [\mathbf{b}_{\mathbb{R}}]_1^2 = [\mathbf{b}_{\mathbb{R}}]_b^2 \text{ for } b = 2, \ldots, 2B. \end{aligned} \tag{39}$$

If $\psi = 1$ then $\mathbf{b}_{\mathbb{R}}$ is the solution to (39); if $\psi = -1$ then $-\mathbf{b}_{\mathbb{R}}$ is the solution. Next, let the $(2B+1)\times(2B+1)$ matrix $\mathbf{T}_{\mathbb{R}}$ be defined as follows:

$$\mathbf{T}_{\mathbb{R}} = \begin{bmatrix} \mathbf{H}_{\mathbb{R}}^T\mathbf{H}_{\mathbb{R}} + \frac{UN_0}{P}\mathbf{I}_{2B} & -\mathbf{H}_{\mathbb{R}}^T\mathbf{s}_{\mathbb{R}} \\ -\mathbf{s}_{\mathbb{R}}^T\mathbf{H}_{\mathbb{R}} & \|\mathbf{s}_{\mathbb{R}}\|_2^2 \end{bmatrix}. \tag{40}$$

Also, let $\mathbf{B}_{\mathbb{R}} = [\mathbf{b}_{\mathbb{R}}^T\ \psi]^T[\mathbf{b}_{\mathbb{R}}^T\ \psi]$. Following steps similar to those in [54], we rewrite the objective function in (39) as

$$\|\psi\mathbf{s}_{\mathbb{R}} - \mathbf{H}_{\mathbb{R}}\mathbf{b}_{\mathbb{R}}\|_2^2 + \frac{UN_0}{P}\|\mathbf{b}_{\mathbb{R}}\|_2^2 = [\mathbf{b}_{\mathbb{R}}^T\ \psi]\mathbf{T}_{\mathbb{R}}[\mathbf{b}_{\mathbb{R}}^T\ \psi]^T = \operatorname{tr}(\mathbf{T}_{\mathbb{R}}\mathbf{B}_{\mathbb{R}})\,. \tag{41}$$

Here, in the last step, we used basic properties of the trace operator. The problem (39) can now be reformulated as

$$\begin{aligned} \underset{\mathbf{B}_{\mathbb{R}}\in\mathbb{S}^{2B+1}}{\text{minimize}} \quad & \operatorname{tr}(\mathbf{T}_{\mathbb{R}}\mathbf{B}_{\mathbb{R}}) \\ \text{subject to} \quad & [\mathbf{B}_{\mathbb{R}}]_{1,1} = [\mathbf{B}_{\mathbb{R}}]_{b,b} \text{ for } b = 2, \ldots, 2B, \\ & [\mathbf{B}_{\mathbb{R}}]_{2B+1,\,2B+1} = 1,\ \mathbf{B}_{\mathbb{R}} \succeq \mathbf{0},\ \text{and}\ \operatorname{rank}(\mathbf{B}_{\mathbb{R}}) = 1. \end{aligned} \tag{42}$$

Here, $\mathbb{S}^{2B+1}$ denotes the set of real and symmetric $(2B+1)\times(2B+1)$ matrices. To see why (39) and (42) are equivalent, remember that $\mathbf{B}_{\mathbb{R}} = [\mathbf{b}_{\mathbb{R}}^T\ \psi]^T[\mathbf{b}_{\mathbb{R}}^T\ \psi]$, which implies that $\mathbf{B}_{\mathbb{R}}$ has rank 1 and that $[\mathbf{B}_{\mathbb{R}}]_{b,b} = [\mathbf{b}_{\mathbb{R}}]_b^2$ for $b = 1, \ldots, 2B$, and that $[\mathbf{B}_{\mathbb{R}}]_{2B+1,2B+1} = \psi^2 = 1$.

Unfortunately, the rank-1 constraint in (42) is nonconvex, which makes this problem just as hard to solve as the original QP problem in (33). Nevertheless, we can use SDR to relax the problem in (42) by omitting the rank-1 constraint, which results in the following SDP:

$$\text{(SDR-QP)} \quad \begin{cases} \underset{\mathbf{B}_{\mathbb{R}}\in\mathbb{S}^{2B+1}}{\text{minimize}} \quad & \operatorname{tr}(\mathbf{T}_{\mathbb{R}}\mathbf{B}_{\mathbb{R}}) \\ \text{subject to} \quad & [\mathbf{B}_{\mathbb{R}}]_{1,1} = [\mathbf{B}_{\mathbb{R}}]_{b,b} \text{ for } b = 2, \ldots, 2B \\ & [\mathbf{B}_{\mathbb{R}}]_{2B+1,\,2B+1} = 1 \text{ and } \mathbf{B}_{\mathbb{R}} \succeq \mathbf{0}. \end{cases} \tag{43}$$

This problem can be solved efficiently using standard methods from convex optimization [58]. If the solution matrix $\mathbf{B}_{\mathbb{R}}^{\text{SDR-QP}}$ has rank one, then SDR finds the exact solution to the problem (QP) in (38). If, however, the rank exceeds one, we have to extract a precoding vector that belongs to the discrete set $\mathcal{X}^B$. As commonly done, one can obtain such a vector by first performing an eigenvalue-decomposition of $\mathbf{B}_{\mathbb{R}}^{\text{SDR-QP}}$ and by then quantizing the first $2B$ entries of the leading eigenvector $\mathbf{u}_{\mathbb{R}}$,

$$\left[\mathbf{x}_{\mathbb{R}}^{\text{SDR-QP}}\right]_b = \sqrt{\frac{P}{2B}}\,\text{sgn}([\mathbf{u}_{\mathbb{R}}]_{2B+1})\,\text{sgn}([\mathbf{u}_{\mathbb{R}}]_b)\,, \quad b = 1, \ldots, 2B. \tag{44}$$

The multiplication by $\text{sgn}([\mathbf{u}_{\mathbb{R}}]_{2B+1})$ takes into account the potential sign change caused by ψ. The resulting complex-valued precoded vector is obtained as follows:

$$\left[\mathbf{x}^{\text{SDR-QP}}\right]_b = \left[\mathbf{x}_{\mathbb{R}}^{\text{SDR-QP}}\right]_b + j\left[\mathbf{x}_{\mathbb{R}}^{\text{SDR-QP}}\right]_{B+b}, \quad b = 1, \ldots, B. \tag{45}$$

We refer to this approach as SDR with a rank-one approximation (SDR1). Alternatively, we can obtain a precoding vector in $\mathcal{X}^B$ using more sophisticated randomized procedures; see the survey article [54] for more details. We refer to this approach as SDR with randomization (SDRr).

SDR enables the computation of approximate solutions to the NP-hard problem (QP) in polynomial time. Specifically, the worst-case complexity scales with $B^{4.5}$ [54]. However, SDR lifts the problem to a higher dimension: from $2B$ dimensions to $(2B + 1)^2$ dimensions. Furthermore, implementing the corresponding numerical solvers entails high hardware complexity [59]. Recently, a hardware-friendly *approximate* SDR solver for problems of dimension up to $B = 16$ was proposed in [59]. However, the associated complexity still prevents its use for massive MU-MIMO systems with hundreds of antennas. Hence, we conclude that SDR is a suitable technique only for small to moderately-sized systems (e.g., 16 BS antennas or less). For larger antenna arrays, alternative methods are necessary. One such method is described next.

B. *Squared ℓ_∞-Norm Relaxation*

We next present a novel method to approximately solving (33), which avoids lifting the problem to a higher dimension and requires low complexity. We start by rewriting the real-valued optimization problem (38) as

$$\begin{aligned} \underset{\mathbf{b}_{\mathbb{R}} \in \mathbb{R}^{2B}}{\text{minimize}} \quad & \|\mathbf{s}_{\mathbb{R}} - \mathbf{H}_{\mathbb{R}}\mathbf{b}_{\mathbb{R}}\|_2^2 + \frac{2BUN_0}{P}\|\mathbf{b}_{\mathbb{R}}\|_\infty^2 \\ \text{subject to} \quad & [\mathbf{b}_{\mathbb{R}}]_1^2 = [\mathbf{b}_{\mathbb{R}}]_b^2 \text{ for } b = 2,\, ,\ldots,\, 2B \end{aligned} \tag{46}$$

where we used that $\|\mathbf{b}_{\mathbb{R}}\|_2^2 = 2B\|\mathbf{b}_{\mathbb{R}}\|_\infty^2$ under the constraint that $[\mathbf{b}_{\mathbb{R}}]_1^2 = [\mathbf{b}_{\mathbb{R}}]_b^2$ for $b = 2,\, \ldots,\, 2B$. By dropping the nonconvex constraints $[\mathbf{b}_{\mathbb{R}}]_1^2 = [\mathbf{b}_{\mathbb{R}}]_b^2$ for $b = 2,\, \ldots,\, 2B$, we obtain the following convex relaxation of (46):

$$(\ell_\infty^2\text{-QP}) \quad \underset{\mathbf{b}_\mathbb{R}\in\mathbb{R}^{2B}}{\text{minimize}} \; \|\mathbf{s}_\mathbb{R} - \mathbf{H}_\mathbb{R}\mathbf{b}_\mathbb{R}\|_2^2 + \frac{2BUN_0}{P}\|\mathbf{b}_\mathbb{R}\|_\infty^2 \tag{47}$$

which, as we shall see, can be solved efficiently. To extract a feasible precoding vector $\mathbf{x}^{\ell_\infty^2\text{-QP}} \in \mathcal{X}^B$ from the solution $\mathbf{b}_\mathbb{R}^{\ell_\infty^2\text{-QP}}$ to the problem (47), we quantize the entries of the vector to the quaternary set $\mathcal{X}$ by computing

$$\left[\mathbf{x}_\mathbb{R}^{\ell_\infty^2\text{-QP}}\right]_b = \sqrt{\frac{P}{2B}}\,\mathrm{sgn}\!\left(\left[\mathbf{b}_\mathbb{R}^{\ell_\infty^2\text{-QP}}\right]_b\right), \quad b = 1,\ldots,2B. \tag{48}$$

As in (45), we then obtain the complex-valued precoded vector as follows:

$$\left[\mathbf{x}^{\ell_\infty^2\text{-QP}}\right]_b = \left[\mathbf{x}_\mathbb{R}^{\ell_\infty^2\text{-QP}}\right]_b + j\left[\mathbf{x}_\mathbb{R}^{\ell_\infty^2\text{-QP}}\right]_{B+b}, \quad b = 1,\ldots,B. \tag{49}$$

There exist several numerical optimization methods that are capable of solving problems of the form of (ℓ_∞^2-QP) in (47) in a computationally efficient manner. The most prominent methods are forward-backward splitting (FBS) [60], [61] and Douglas-Rachford (DR) splitting [62], [63]. In what follows, we develop a DR splitting method, which we refer to as squared-infinity norm Douglas-Rachford splitting (SQUID). We define the two convex functions $g(\mathbf{b}_\mathbb{R}) = \|\mathbf{s}_\mathbb{R} - \mathbf{H}_\mathbb{R}\mathbf{b}_\mathbb{R}\|_2^2$ and $f(\mathbf{b}_\mathbb{R}) = \frac{2BUN_0}{P}\|\mathbf{b}_\mathbb{R}\|_\infty^2$, and solve

$$\underset{\mathbf{b}_\mathbb{R}\in\mathbb{R}^{2B}}{\text{minimize}} \; g(\mathbf{b}_\mathbb{R}) + f(\mathbf{b}_\mathbb{R}). \tag{50}$$

Let

$$\mathrm{prox}_h(\mathbf{w}) = \underset{\mathbf{b}_\mathbb{R}\in\mathbb{R}^{2B}}{\arg\min}\, h(\mathbf{b}_\mathbb{R}) + \tfrac{1}{2}\|\mathbf{b}_\mathbb{R} - \mathbf{w}\|_2^2 \tag{51}$$

define the proximal operator for the function $h(\cdot)$ [60]. By initializing $\mathbf{b}_\mathbb{R}^{(0)} = \mathbf{0}_{2B\times 1}$ and $\mathbf{c}_\mathbb{R}^{(0)} = \mathbf{0}_{2B\times 1}$, SQUID performs the following iterative procedure for $t = 1, 2, \ldots$ until convergence or until a maximum number of iterations has been reached:

$$\mathbf{a}_\mathbb{R}^{(t)} = \mathrm{prox}_g(2\mathbf{b}_\mathbb{R}^{(t-1)} - \mathbf{c}_\mathbb{R}^{(t-1)}) \tag{52}$$

$$\mathbf{b}_\mathbb{R}^{(t)} = \mathrm{prox}_f(\mathbf{c}_\mathbb{R}^{(t-1)} - \mathbf{a}_\mathbb{R}^{(t)} - \mathbf{b}_\mathbb{R}^{(t-1)}) \tag{53}$$

$$\mathbf{c}_\mathbb{R}^{(t)} = \mathbf{c}_\mathbb{R}^{(t-1)} + \mathbf{a}_\mathbb{R}^{(t)} - \mathbf{b}_\mathbb{R}^{(t-1)}. \tag{54}$$

Algorithm 1 Proximal operator for the ℓ_∞^2-norm

inputs: $\mathbf{z} \in \mathbb{R}^N$, $\lambda \in (0, \infty)$
$\mathbf{a} \leftarrow \mathrm{abs}(\mathbf{z})$
$\mathbf{s} \leftarrow \mathrm{sort}(\mathbf{a}, \text{`descending'})$
for $k = 1, \ldots, N$ **do**
    $c_k \leftarrow \frac{1}{2\lambda+k} \sum_{i=1}^{k} s_i$
end for
$\alpha \leftarrow \max\left\{0, \max_k\{c_k\}\right\}$
for $k = 1, \ldots, N$ **do**
    $u_k \leftarrow \min\{a_k, \alpha\}\,\mathrm{sgn}(z_k)$
end for
return $\mathbf{u}$

The proximal operator $\mathrm{prox}_g(\cdot)$ in (52) has the following simple[6] expression:

$$\mathrm{prox}_g(\mathbf{w}) = (\mathbf{H}_\mathbb{R}^T\mathbf{H}_\mathbb{R} + \tfrac{1}{2}\mathbf{I}_{2B\times 2B})^{-1}(\mathbf{H}_\mathbb{R}^T\mathbf{s}_\mathbb{R} + \tfrac{1}{2}\mathbf{w}). \tag{55}$$

While the proximal operator for the ℓ_∞-norm is well known in the literature [60], the proximal operator $\mathrm{prox}_f(\cdot)$ for the *squared* ℓ_∞-norm, needed in (53), appears to be novel. The following theorem details an efficient procedure for computing this proximal operator. The proof is given in Appendix B.

Theorem 4: Let $\lambda > 0$. Then, the squared ℓ_∞-norm proximal operator

$$\mathbf{u} = \mathrm{prox}_{\lambda\ell_\infty^2}(\mathbf{z}) = \arg\min_{\mathbf{u}\in\mathbb{R}^N} \lambda\|\mathbf{u}\|_\infty^2 + \tfrac{1}{2}\|\mathbf{z}-\mathbf{u}\|_2^2 \tag{56}$$

can be computed using the procedure summarized in Algorithm 1.

In summary, SQUID enables us to solve the relaxed problem in (47) in a computationally efficient manner. Indeed, each iteration requires only simple matrix and vector operations, and the evaluation of the proximal operator in Algorithm 1. The performance of SQUID is investigated in Section V where we demonstrate that this low-complexity algorithm achieves performance that is comparable to the performance of SDR, which is far more demanding in terms of computational complexity.

C. Sphere Precoding

Sphere decoding (SD) is a common method to solve CVPs exactly but at lower average computational complexity than a naïve exhaustive search [51], [52], [64]. The idea of SD is to constrain the search for possible optimal solutions to a hypersphere of radius r. By transforming the optimal CVP into a tree-search problem, one can then perform a depth-first branch-and-bound procedure and prune branches that exceed

[6] One can further accelerate the evaluation of this proximal operator by using the Woodbury matrix identity (which reduces the dimension of the matrix inverse), and by precomputing certain constant quantities, such as $\mathbf{H}_\mathbb{R}^T\mathbf{s}_\mathbb{R}$.

the radius constraint to reduce the number of candidate vectors. While SD reduces (often significantly) the average complexity (compared to an exhaustive search), it was shown to exhibit exponential complexity in the number of variables for data detection in multi-antenna wireless systems [65], [66].

To adapt SD to 1-bit quantized precoding (we call this adaptation *sphere precoding* (SP)), we proceed as follows. Assume that the optimal precoding factor β is known. Then, we can rewrite the objective function in (35) as follows:

$$\|\mathbf{s}-\beta\mathbf{H}\mathbf{x}\|_2^2+\beta^2 UN_0 \overset{(a)}{=} \|\mathbf{s}-\beta\mathbf{H}\mathbf{x}\|_2^2+\beta^2\frac{UN_0}{P}\|\mathbf{x}\|_2^2 \overset{(b)}{=} \left\|\bar{\mathbf{s}}-\beta\overline{\mathbf{H}}\mathbf{x}\right\|_2^2. \tag{57}$$

In (a), we used that $\|\mathbf{x}\|_2^2 = P$ in the 1-bit case; in (b) we set $\bar{\mathbf{s}} = [\mathbf{s}^T\ \mathbf{0}_B^T]^T$ and $\overline{\mathbf{H}} = [\mathbf{H}^T\ \sqrt{UN_0/P}\,\mathbf{I}_B]^T$. Hence, we can write the precoding problem as

$$\underset{\mathbf{x}\in\mathcal{X}^B}{\text{minimize}}\ \left\|\bar{\mathbf{s}}-\beta\overline{\mathbf{H}}\mathbf{x}\right\|_2 \tag{58}$$

which can be solved using SD. More specifically, by computing the QR factorization $\overline{\mathbf{H}} = \mathbf{Q}\mathbf{R}$, where $\mathbf{Q}\in\mathbb{C}^{(U+B)\times B}$ with $\mathbf{Q}^H\mathbf{Q} = \mathbf{I}_B$ and $\mathbf{R}\in\mathbb{C}^{B\times B}$ is upper triangular with non-negative diagonal entries, we obtain the equivalent problem

$$\text{(SP)}\quad \underset{\mathbf{x}\in\mathcal{X}^B}{\text{minimize}}\ \left\|\mathbf{Q}^H\bar{\mathbf{s}}-\beta\mathbf{R}\mathbf{x}\right\|_2. \tag{59}$$

The triangular structure of this problem allows us to deploy standard SD methods, as the one in [51].

In practice, the optimal precoding factor β is unknown. We therefore propose the following alternating optimization approach. At iteration $t = 1$, we initialize the algorithm with the precoding factor obtained from WF precoding. Specifically, we use (34) and set $\beta_1 = \hat{\beta}(\mathbf{x}^{\text{WF}})$. We then solve (SP) to obtain $\mathbf{x}_t^{\text{SP}}$ and compute an improved precoding factor $\beta_{t+1} = \hat{\beta}(\mathbf{x}_t^{\text{SP}})$ using (34). We repeat this procedure for $t = 2, 3, \ldots$ until convergence or until a maximum number of iterations is reached. Our simulations have shown that this procedure usually converges in only 1-to-3 iterations and achieves near-optimal performance for small to moderately-sized systems MIMO systems (in Section V-A, we present numerical results for the case of $B = 8$ antennas). We note that a plethora of SD-related methods can be used to solve SP. However, the exponential complexity of SD prevents its use for massive MIMO systems with hundreds of antennas.

D. Decoding at the UEs

As for the case of linear-quantized precoders, we assume that each UE is able to scale the received signal by β_u. Note that the scaling factor β_u can not be chosen to be equal to β, since β depends in the nonlinear case on the transmit vector s. It is worth noting that for the special case in which the entries of s are points of a constant-modulus constellation (e.g., M-PSK) and the receiver employs symbol-wise

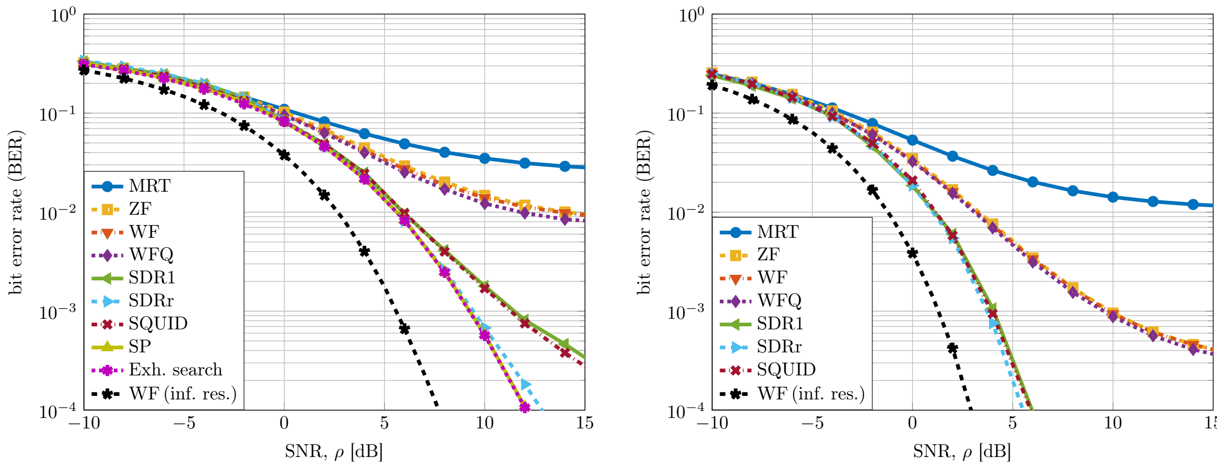

(a) $B = 8$ and $U = 2$.

(b) $B = 128$ and $U = 16$.

Fig. 3. Uncoded BER with QPSK signaling for 1-bit DACs as a function of the SNR, ρ, for the precoders introduced in Section III and in Section IV. The performance of the WFQ precoder proposed in [29] is also illustrated for comparison.

nearest-neighbor decoding (i.e., each UE maps its estimate $\hat{s}_u$ in (3) to the nearest constellation point, which implies that the residual MUI and quantization errors are treated as Gaussian noise, although they are non-Gaussian), the scaling value chosen by the receiver does not affect performance, because the decision regions are circular sectors. In the simulation results in Section V, we shall focus exactly on this setup.

V. Numerical Results

We will now present numerical simulation results for the quantized precocers introduced in Section III and Section IV. Due to space constraints, we shall focus on a limited set of system parameters.[7]

A. Error-Rate Performance

We start by comparing the performance of the developed precoders in terms of uncoded bit error rate (BER). In what follows, we assume that the UEs perform symbol-wise nearest-neighbor decoding.

In Fig. 3, we compare the BER with QPSK signaling and 1-bit DACs for the linear precoders presented in Section III (namely, WF, ZF and, MRT) and the nonlinear precoding algorithms presented in Section IV (namely, SDR1, SDRr, SQUID and SP). For comparison, we also report the performance of the WF-quantized (WFQ) precoder proposed in [29], and the performance of the WF precoder for the infinite-resolution case.

[7]Our simulation framework will be made available for download from GitHub after (possible) acceptance of the paper. This will enable interested readers to perform simulations with different system parameters and also to evaluate alternative precoding algorithms.

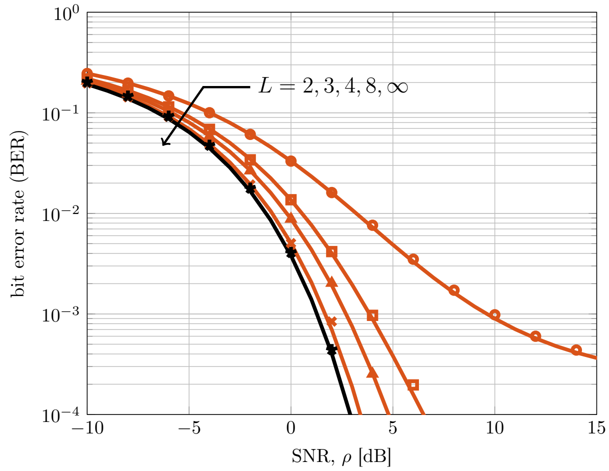

Fig. 4. Uncoded BER with QPSK signaling and WF precoding with multi-bit DACs; $B = 128$ and $U = 16$. Here, L denotes the number of quantization levels. The markers correspond to simulated values and the solid lines correspond to closed-form approximations.

In Fig. 3a, we consider the case $B = 8$ BS antennas and $U = 2$ UEs (moderately-sized MIMO system). For this case, one can find the optimal solution to (QP) in (33) by exhaustive search. We find that the gap between the performance of the optimal nonlinear precoder and the performance of infinite-resolution WF precoder is remarkably small: about 4 dB for a target BER of 10^{-3}. Furthermore, the SP algorithm achieves near-optimal performance, as does SDRr. SQUID and SDR1 closely follow the optimal curve up to a BER of 10^{-2} but then their performance degrades. The linear-quantized precoders, on the other hand, are adversely impacted by the coarse 1-bit quantization. Indeed, the BER for linear-quantized precoding saturates at 10^{-2} or above. Hence, in contrast to recently reported findings [31], our results suggest that nonlinear precoding offers significant advantages in terms of BER compared to linear-quantized precoding.

In Fig. 3b, we consider a massive MIMO system with $B = 128$ BS antennas and $U = 16$ UEs. Exhaustive search and SP are not viable in this setup due to the exponential complexity in B that these methods entail. We note that the increased number of antennas yields a performance improvement for the linear-quantized precoders. Indeed, with ZF, WF, or WFQ, one can support error probabilities below 10^{-3}. However, the nonlinear precoders still significantly outperform the linear-quantized precoders. The gap to the infinite-resolution BER with SQUID is about 3 dB for a target BER of 10^{-3}; with WFQ precoding, the gap is about 8 dB for the same BER target.

In Fig. 4, we show the uncoded BER for WF precoding as a function of the SNR and the number of DAC levels L for a system with $U = 16$ UEs and $B = 128$ BS antennas. The simulated BER values in Fig. 4 are compared with closed-form approximations obtained by approximating the uncoded BER by $1 - \Phi\left(\sqrt{\bar{\gamma}^{\text{WF}}}\right)$ where $\bar{\gamma}^{\text{WF}}$ is given in (30). We observe that this approximation is accurate for the

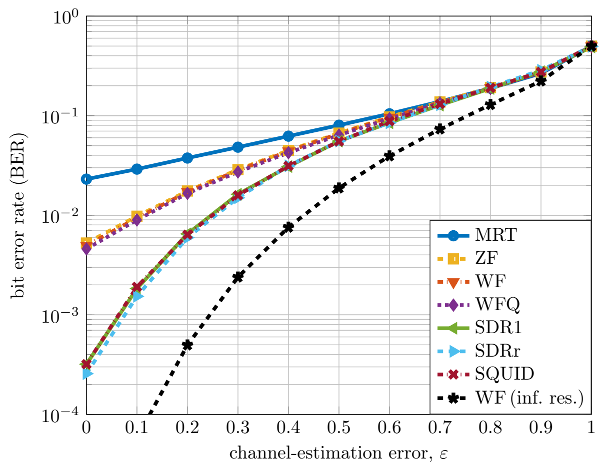

Fig. 5. Uncoded BER with QPSK signaling for 1-bit DACs as a function of the channel-estimation error, ε.

entire range of SNR values. We further observe that low BER probabilities can be attained with very coarse DACs. Interestingly, by only adding a zero-level in the DACs (so that $L = 3$), the performance is drastically improved compared to the 1-bit case ($L = 2$). Furthermore, with only 3-bit DACs ($L = 8$) the performance gap to the infinite-resolution case is negligible. This suggests that it is possible to significantly reduce the number of bits in the high-resolution DACs used in today's systems.

B. Robustness to Channel-Estimation Errors

So far, we have assumed that the BS has access to perfect CSI. In this section we shall relax this assumption to investigate the robustness of the developed algorithms to channel estimation errors. More specifically, we shall assume that the BS has access to a noisy version of $\mathbf{H}$ modelled as

$$\widehat{\mathbf{H}} = \sqrt{1-\varepsilon}\mathbf{H} + \sqrt{\varepsilon}\mathbf{Z}. \tag{60}$$

Here, $\varepsilon \in [0, 1]$ and $\mathbf{Z}$ has $\mathcal{CN}(0, 1)$ entries. We refer to ε as the channel-estimation error: $\varepsilon = 0$ corresponds to perfect CSI and $\varepsilon = 1$ corresponds to no CSI; intermediate values corresponds to partial CSI.

In Fig. 5, we show, for the 1-bit case, the uncoded BER with QPSK signaling as a function of the channel-estimation error ε for a system with $B = 128$ BS antennas and $U = 16$ UEs. Interestingly, the nonlinear precoders still outperform the linear-quantized precoders for $\varepsilon \leq 0.5$. This implies that nonlinear precoders can be used also when only imperfect CSI is available to the BS.

C. Achievable rate

Next, we validate the analytic results on the achievable rate with linear-quantized precoders reported in Section III by numerical simulations.

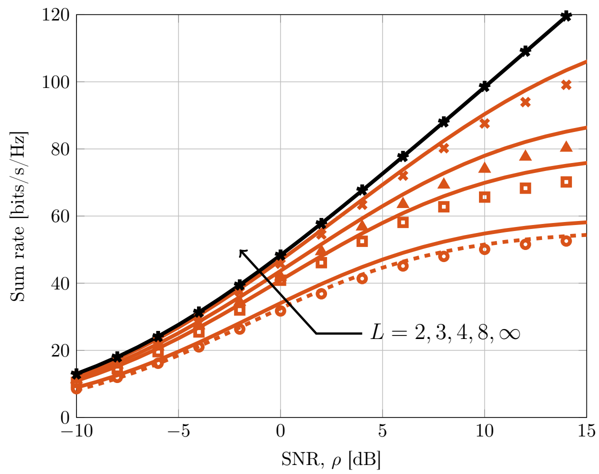

Fig. 6. Achievable sum-rate with Gaussian signaling and WF precoding with multi-bit DACs; $B = 128$ and $U = 16$. Here, L denotes the number of quantization levels. The markers correspond to simulated values and the solid lines correspond to closed-form approximations. The dashed line corresponds to the lower bound (23) for 1-bit DACs.

In Fig. 6, we show the achievable sum-rate with Gaussian signaling and WF precoding as a function of the SNR and the number of DAC levels. The rate approximation computed using (30) is illustrated together with the rate lower bound (23) for the 1-bit case. We also show the achievable rate computed numerically using (21) by simulating many noise and interference realizations for each channel realization and by mapping the resulting $\hat{s}_u$ to a rectangular grid in the complex plane to estimate the probability density functions required to compute (21) (see, e.g., [67] for details). We note that the asymptotic approximation matches well the numerical results, confirming its accuracy. We further note that, analogously to the uplink scenario [22], [23], high sum-rate throughputs can be achieved despite having low-resolution DACs at the BS.

VI. Conclusions

We have presented novel algorithms for the problem of downlink precoding for massive MIMO systems equipped with low-resolution DACs at the BS. To handle the challenges imposed by the finite-cardinality outputs from the DACs, we have considered two distinct approaches, namely linear-quantized precoding for Q-bit DACs, and nonlinear precoding algorithms for 1-bit DACs.

We have simulated the performance for a downlink massive MIMO system operating over a frequency-flat Rayleigh-fading channel, whose realizations are known perfectly at the BS. We have shown that, with linear-quantized precoding, DACs with 3-to-4 bits resolution are sufficient to close the gap to the performance (measured in terms of both BER and achievable rate) obtained with infinite-resolution DACs. Furthermore, we have developed an asymptotic approximation of the effective SINDR, which can be used to predict the system performance accurately using simple closed-form expressions.

Linear-quantized precoders are, however, far from optimal. For the case of 1-bit DACs, we have shown that the error-rate performance can be significantly improved by allowing for nonlinear precoding algorithms. For example, we showed that for a system with 128 BS antennas serving 16 UEs, the gap to infinite-resolution performance is about 3 dB for a target BER of 10^{-3}. Nonlinear precoding, however, entails increased signal-processing complexity. For small-to-moderate sized systems (e.g., 16 BS antennas or less), SDR- and SP-based precoders offer near-optimal BER-performance at tolerable complexity. For massive MIMO systems, SQUID is an efficient and hardware-friendly algorithm to find a near-optimal solution to the 1-bit quantized precoding problem.

APPENDIX A
PROOF OF THEOREM 2

Let $\mathbf{z} = \mathbf{P}\mathbf{s} \in \mathbb{C}^B$. It follows from Theorem 1 that the covariance matrices $\mathbf{C}_{\mathbf{xz}} = \mathbb{E}_{\mathbf{s}}\left[\mathbf{x}\mathbf{z}^H\right]$ and $\mathbf{C}_{\mathbf{zz}} = \mathbb{E}_{\mathbf{s}}\left[\mathbf{z}\mathbf{z}^H\right]$ are related as follows:

$$\mathbf{C}_{\mathbf{xz}} = \mathbf{G}\mathbf{C}_{\mathbf{zz}} \tag{61}$$

where $\mathbf{G}$ is a $B \times B$ diagonal matrix with

$$[\mathbf{G}]_{b,b} = \frac{1}{\sigma_b^2}\,\mathbb{E}[\mathcal{Q}(z_b)z_b^*] \tag{62}$$

where $z_b = [\mathbf{z}]_b$ and $\sigma_b^2 = \mathbb{E}\left[|z_b|^2\right]$ for $b = 1, \dots, B$. Note now that

$$\mathbf{C}_{\mathbf{zz}} = \mathbb{E}_{\mathbf{s}}\left[\mathbf{z}\mathbf{z}^H\right] = \mathbf{P}\,\mathbb{E}_{\mathbf{s}}\left[\mathbf{s}\mathbf{s}^H\right]\mathbf{P}^H = \mathbf{P}\mathbf{P}^H. \tag{63}$$

It follows from (61) that we can write the quantized signal as $\mathbf{x} = \mathbf{G}\mathbf{z} + \mathbf{d}$, where the distortion $\mathbf{d}$ is uncorrelated with $\mathbf{z}$. Indeed, note that

$$\mathbb{E}_{\mathbf{s}}\left[\mathbf{d}\mathbf{z}^H\right] = \mathbb{E}_{\mathbf{s}}\left[(\mathbf{x} - \mathbf{G}\mathbf{z})\mathbf{z}^H\right] = \mathbf{C}_{\mathbf{xz}} - \mathbf{G}\mathbf{C}_{\mathbf{zz}} = \mathbf{0}_{B\times B} \tag{64}$$

where the last equality follows from (61). We next evaluate (62). Note that, since the real and imaginary components of the symbol vector $\mathbf{s}$ are independent and identically distributed, so are the real and imaginary components of the precoded vector $\mathbf{z}$. Therefore, it holds that $\mathbb{E}[\mathcal{Q}(z_b)z_b^*] = 2\,\mathbb{E}[\mathcal{Q}(z)z]$, where we have introduced the random variable $z \sim \mathcal{N}(0, \sigma_b^2/2)$. For a uniform DAC, the quantizer-mapping function can be expressed as

$$\mathcal{Q}(z) = \frac{\alpha\Delta}{2}(1 - L) + \alpha\Delta\sum_{i=1}^{L-1}\mathbb{1}_{\left[\Delta\left(i-\frac{L}{2}\right),\infty\right)}(z). \tag{65}$$

Hence, we have that

$$[\mathbf{G}]_{b,b} = \frac{2\alpha\Delta}{\sigma_b^2}\sum_{i=1}^{L-1}\int_{\Delta\left(i-\frac{L}{2}\right)}^{\infty}\frac{z}{\sqrt{\pi\sigma_b^2}}\exp\!\left(-\frac{z^2}{\sigma_b^2}\right)dz = \frac{\alpha\Delta}{\sqrt{\pi\sigma_b^2}}\sum_{i=1}^{L-1}\exp\!\left(-\frac{\Delta^2}{\sigma_b^2}\left(i-\frac{L}{2}\right)^2\right). \quad (66)$$

The desired result (14) follows from (66) by using that $\sigma_b^2 = [\mathbf{P}\mathbf{P}^H]_{b,b}$.

Appendix B
Proof of Theorem 4

We start by rewriting the proximal operator in (56) as

$$\mathbf{u} = \underset{\mathbf{x}\in\mathbb{R}^N,\ \alpha\in\mathbb{R}}{\arg\min}\ \lambda\alpha^2 + \frac{1}{2}\|\mathbf{x}-\mathbf{y}\|_2^2 \quad \text{subject to } x_k^2 \leq \alpha^2, \quad k = 1,\ldots,N \quad (67)$$

and use the Karush-Kuhn-Tucker (KKT) conditions [58] to compute its solution. The Lagrangian of the optimization problem in (67) is given by

$$\mathcal{L}(\mathbf{x},\alpha,\mathbf{u}) = \lambda\alpha^2 + \frac{1}{2}\|\mathbf{x}-\mathbf{y}\|_2^2 + \sum_{k=1}^{N} u_k(x_i^2 - \alpha^2) \quad (68)$$

which yields the following two stationarity conditions:

$$\lambda - \sum_{k=1}^{N} u_i = 0 \quad (69)$$

$$x_k - y_k + 2x_k u_k = 0, \quad k = 1,\ldots,N. \quad (70)$$

The stationarity condition (70) reveals that $x_k = y_k/(1+2u_k)$, which implies that if $u_k = 0$, then $x_k = y_k$. Complementary slackness yields $u_k(x_k^2 - \alpha_k^2) = 0$, which implies that if $u_k \neq 0$, then $x_k^2 = \alpha^2$ for a given k. Hence the values of x_k must either be $|x_k| = \alpha$ or $x_k = y_k$ so that $|x_k| < \alpha$. In words, the proximal operator in (67) clips to $x_k = \mathrm{sgn}(y_k)\alpha$ the values y_k whose magnitude exceeds α and leaves the remaining values unaffected. Hence, we only need to determine the optimal clipping threshold $\alpha^* > 0$.

Assume $x_k \neq 0$ without loss of generality (in the case $y_k = 0$, we have $x_k = 0$). Then, the stationarity condition in (70) reveals that $u_k = \frac{1}{2}\left(\frac{y_k}{x_k} - 1\right)$. Together with the stationarity condition (69), we have

$$\sum_{k=1}^{N} u_k = \frac{1}{2}\sum_{k=1}^{N}\left(\frac{y_k}{x_k} - 1\right) = \lambda \quad (71)$$

which implies that

$$\sum_{k=1}^{N}\frac{y_k}{x_k} = 2\lambda + N. \quad (72)$$

We now partition the indices $k = 1, \dots, N$ into two disjoint sets Ω and Ω^c, The set Ω contains the indices of the entries y_k for which $|y_k| \geq \alpha$; the set Ω^c contains the indices of the entries u_k for which $|y_k| < \alpha$. Since $x_k = \mathrm{sgn}(y_k)\alpha$ for $k \in \Omega$ and $x_k = y_k$ for $k \in \Omega^c$, it follows from (72) that

$$\sum_{k\in\Omega} \frac{|y_k|}{\alpha} + \sum_{k\in\Omega^c} 1 = 2\lambda + N. \tag{73}$$

Hence,

$$\sum_{k\in\Omega} \frac{|y_k|}{\alpha} = 2\lambda + N - |\Omega^c| = 2\lambda + |\Omega|. \tag{74}$$

We see from (74) that the clipping threshold α must satisfy

$$\alpha = \frac{\sum_{k\in\Omega} |y_k|}{2\lambda + |\Omega|}. \tag{75}$$

To solve (67), it is convenient to sort the values $|y_k|$ in descending order. Specifically, let us denote these values by $r_1 \geq r_2 \geq \cdots \geq r_N$. Then one computes $\alpha_\ell = \sum_{k=1}^{\ell} r_k/(2\lambda + \ell)$ for $\ell = 1, 2, \dots, N$ and chooses α^* as the only α_ℓ that satisfies $r_{\ell+1} < \alpha_\ell \leq r_\ell$. Simple algebraic manipulations reveal that this is equivalent to setting $\alpha^* = \max_\ell \alpha_\ell$. We then use α^* to perform element-wise clipping. Algorithm 1 implements exactly this procedure in a computationally efficient manner.

References

[1] F. Rusek, D. Persson, B. Kiong, E. G. Larsson, T. L. Marzetta, O. Edfors, and F. Tufvesson, "Scaling up MIMO: Oppurtunities and challenges with very large large arrays," *IEEE Signal Process. Mag.*, vol. 30, no. 1, pp. 40–60, Jan. 2013.

[2] E. G. Larsson, F. Tufvesson, O. Edfors, and T. L. Marzetta, "Massive MIMO for next generation wireless systems," *IEEE Commun. Mag.*, vol. 52, no. 2, pp. 186–195, Feb. 2014.

[3] L. Lu, G. Ye Li, A. L. Swindlehurst, A. Ashikhmin, and R. Zhang, "An overview of massive MIMO: Benefits and challenges," *IEEE J. Sel. Topics Signal Process.*, vol. 8, no. 5, pp. 742–758, Oct. 2014.

[4] G. Caire and S. Shamai (Shitz), "On the achievable throughput of a multiantenna Gaussian broadcast channel," *IEEE Trans. Inf. Theory*, vol. 49, no. 7, pp. 1691–1706, Jul. 2003.

[5] W. Yu and J. M. Cioffi, "Sum capacity of Gaussian vector broadcast channels," *IEEE Trans. Inf. Theory*, vol. 50, no. 9, pp. 1875–1892, Sep. 2004.

[6] S. Viswanath, N. Jindal, and A. Goldsmith, "Duality, achievable rates, and sum-rate capacity of Gaussian MIMO broadcast channels," *IEEE Trans. Inf. Theory*, vol. 49, no. 10, pp. 2658–2668, Oct. 2003.

[7] P. Viswanath and D. Tse, "Sum capacity of the vector Gaussian broadcast channel and uplink–downlink duality," *IEEE Trans. Inf. Theory*, vol. 49, no. 8, pp. 1912–1921, Aug. 2003.

[8] M. H. Costa, "Writing on dirty paper," *IEEE Trans. Inf. Theory*, vol. 29, no. 3, pp. 439–441, May 1983.

[9] R. D. Wesel and J. M. Cioffi, "Achievable rates for Tomlinson–Harashima precoding," *IEEE Trans. Inf. Theory*, vol. 44, no. 2, pp. 824–831, Mar. 1998.

[10] C. Windpassinger, R. F. H. Fischer, T. Vencel, and J. B. Huber, "Precoding in multiantenna and multiuser communications," *IEEE Trans. Wireless Commun.*, vol. 3, no. 4, pp. 1305–1316, Jul. 2004.

[11] C. Windpassinger, R. F. H. Fischer, and J. B. Huber, "Lattice-reduction-aided broadcast precoding," *IEEE Trans. Commun.*, vol. 52, no. 12, pp. 2057–2060, Dec. 2004.

[12] B. M. Hochwald, C. B. Peel, and A. L. Swindlehurst, "A vector-perturbation technique for near-capacity multiantenna multiuser communication—Part II: Perturbation," *IEEE Trans. Commun.*, vol. 53, no. 3, pp. 537–544, Mar. 2005.

[13] H. Yang and T. L. Marzetta, "Performance of conjugate and zero-forcing beamforming in large-scale antenna systems," *IEEE J. Sel. Areas Commun.*, vol. 31, no. 2, pp. 172–179, Feb. 2013.

[14] H. Q. Ngo, E. G. Larsson, and T. L. Marzetta, "Massive MU-MIMO downlink TDD systems with linear precoding and downlink pilots," in *Proc. Allerton Conf. Commun., Contr., Comput.*, Monticello, IL, Oct. 2013.

[15] C. Studer, M. Wenk, and A. Burg, "MIMO transmission with residual transmit-RF impairments," in *Int. ITG Workshop on Smart Antennas (WSA)*, Bremen, Germany, Feb. 2010, pp. 189–196.

[16] U. Gustavsson, C. Sanchéz-Perez, T. Eriksson, F. Athley, G. Durisi, P. Landin, K. Hausmair, C. Fager, and L. Svensson, "On the impact of hardware impairments on massive MIMO," in *Proc. IEEE Global Telecommun. Conf. (GLOBECOM)*, Austin, TX, Dec. 2014, pp. 294–300.

[17] X. Zhang, M. Matthaiou, M. Coldrey, and E. Björnson, "Impact of residual transmit RF impairments on training-based MIMO systems," *IEEE Trans. Commun.*, vol. 63, no. 8, pp. 2899–2911, Aug. 2015.

[18] F. Athley, G. Durisi, and U. Gustavsson, "Analysis of massive MIMO with hardware impairments and different channel models," in *European Conf. Ant. Prop. (EUCAP)*, Lisbon, Portugal, Apr. 2015.

[19] R. H. Walden, "Analog-to-digital converter survey and analysis," *IEEE J. Sel. Areas Commun.*, vol. 17, no. 4, pp. 539–550, Apr. 1999.

[20] B. Murmann, "ADC performance survey 1997-2015." [Online]. Available: http://web.stanford.edu/~murmann/adcsurvey.html

[21] C. Risi, D. Persson, and E. G. Larsson, "Massive MIMO with 1-bit ADC," Apr. 2014. [Online]. Available: http://arxiv.org/abs/1404.7736

[22] S. Jacobsson, G. Durisi, M. Coldrey, U. Gustavsson, and C. Studer, "One-bit massive MIMO: Channel estimation and high-order modulations," in *Proc. IEEE Int. Conf. Commun. Workshop (ICCW)*, London, U.K., June 2015, pp. 1304–1309.

[23] Y. Li, C. Tao, G. Seco-Granados, A. Mezghani, A. L. Swindlehurst, and L. Liu, "Channel estimation and performance analysis of one-bit massive MIMO systems," Sep. 2016. [Online]. Available: https://arxiv.org/abs/1609.07427

[24] C. Mollén, J. Choi, E. G. Larsson, and R. W. Heath Jr., "Performance of the wideband massive uplink MIMO with one-bit ADCs," Feb. 2016. [Online]. Available: https://arxiv.org/abs/1602.07364

[25] C. Studer and G. Durisi, "Quantized massive MU-MIMO-OFDM uplink," *IEEE Trans. Commun.*, vol. 64, no. 6, pp. 2387–2399, Jun. 2016.

[26] C. Studer and E. G. Larsson, "PAR-aware large-scale multi-user MIMO-OFDM downlink," *IEEE J. Sel. Areas Commun.*, vol. 31, no. 2, pp. 303–313, Feb. 2013.

[27] S. K. Mohammed and E. G. Larsson, "Per-antenna constant envelope precoding for large multi-user MIMO systems," *IEEE Trans. Commun.*, vol. 61, no. 3, pp. 1059–1071, Mar. 2013.

[28] ——, "Constant-envelope multi-user precoding for frequency-selective massive MIMO systems," *IEEE Commun. Lett.*, vol. 2, no. 5, pp. 547–550, Oct. 2013.

[29] A. Mezghani, R. Ghiat, and J. A. Nossek, "Transmit processing with low resolution D/A-converters," in *Proc. IEEE Int. Conf. Electron., Circuits, Syst. (ICECS)*, Yasmine Hammamet, Tunisia, Dec. 2009, pp. 683–686.

[30] R. D. J. Guerreiro and P. Montezuma, "Use of 1-bit digital-to-analogue converters in massive MIMO systems," *IEEE Electron. Lett.*, vol. 52, no. 9, pp. 778–779, Apr. 2016.

[31] A. K. Saxena, I. Fijalkow, and A. L. Swindlehurst, "On one-bit quantized ZF precoding for the multiuser massive MIMO downlink," in *IEEE Sensor Array and Multichannel Signal Process. Workshop (SAM)*, Rio de Janeiro, Brazil, Jul. 2016.

[32] O. B. Usman, H. Jedda, A. Mezghani, and J. A. Nossek, "MMSE precoder for massive MIMO using 1-bit quantization," in *Proc. IEEE Int. Conf. Acoust., Speech, Signal Process. (ICASSP)*, Shanghai, China, Mar. 2016, pp. 3381–3385.

[33] E. Björnson, M. Bengtsson, and B. Ottersten, "Optimal multiuser transmit beamforming: A difficult problem with a simple solution structure," *IEEE Signal Process. Mag.*, vol. 31, no. 4, pp. 142–148, Jul. 2014.

[34] E. Björnson and E. Jorswieck, "Optimal resource allocation in coordinated multi-cell systems," *Foundations and Trends in Communications and Information Theory*, vol. 9, no. 2-3, pp. 113–381, 2013.

[35] S. S. Christensen, E. C. Agarwal, and J. M. Cioffi, "Weighted sum-rate maximization using weighted MMSE for MIMO-BC beamforming design," *IEEE Trans. Wireless Commun.*, vol. 7, no. 12, pp. 4792–4799, Dec. 2008.

[36] M. Joham, W. Utschick, and J. A. Nossek, "Linear transmit processing in MIMO communications systems," *IEEE Trans. Signal Process.*, vol. 53, no. 8, pp. 2700–2712, Aug. 2005.

[37] S. Shi, M. Schubert, and H. Boche, "Downlink MMSE transceiver optimization for multiuser MIMO systems: Duality and sum-MSE minimization," *IEEE Trans. Signal Process.*, vol. 55, no. 11, pp. 5436–5446, Nov. 2007.

[38] J. J. Bussgang, "Crosscorrelation functions of amplitude-distorted Gaussian signals," Res. Lab. Elec., Cambridge, MA, Tech. Rep. 216, Mar. 1952.

[39] D. Hui and D. L. Neuhoff, "Asymptotic analysis of optimal fixed-rate uniform scalar quantization," *IEEE Trans. Inf. Theory*, vol. 47, no. 3, pp. 957–977, Mar. 2001.

[40] N. Al-Dhahir and J. M. Cioffi, "On the uniform ADC bit precision and clip level computation for a Gaussian signal," *IEEE Trans. Signal Process.*, vol. 44, no. 2, pp. 434–438, Feb. 1996.

[41] H. E. Rowe, "Memoryless nonlinearities with Gaussian inputs: Elementary results," *Bell Labs Tech. J.*, vol. 61, no. 7, pp. 1519–1525, Sep. 1982.

[42] H. Q. Ngo and E. G. Larsson, "No downlink pilots are needed in TDD massive MIMO," Sep. 2016. [Online]. Available: https://arxiv.org/abs/1606.02348

[43] D. M. Arnold, H.-A. Loeliger, P. O. Vontobel, A. Kavcic, and W. Zeng, "Simulation-based computation of information rates for channels with memory," *IEEE Trans. Inf. Theory*, vol. 52, no. 8, pp. 3498–3508, Aug. 2006.

[44] J. Scarlett, "Reliable communication under mismatched decoding," Ph.D. dissertation, University of Cambridge, U.K., Jun. 2014.

[45] A. Lapidoth, "Mismatched decoding and the multiple access channel," *IEEE Trans. Inf. Theory*, vol. 42, no. 5, pp. 1439–1452, Sep. 1996.

[46] J. H. Van Vleck and D. Middleton, "The spectrum of clipped noise," *Proc. IEEE*, vol. 54, no. 1, pp. 2–19, Jan. 1966.

[47] G. Jacovitti and A. Neri, "Estimation of the autocorrelation function of complex Gaussian stationary processes by amplitude clipped signals," *IEEE Trans. Inf. Theory*, vol. 40, no. 1, pp. 239–245, Jan. 1994.

[48] R. Coulliet and M. Debbah, *Random Matrix Methods for Wireless Communications*. Cambridge: Cambridge Univ. Press, 2011.

[49] S. Wagner, R. Coulliet, M. Debbah, and D. T. M. Slock, "Large system analysis of linear precoding in correlated MISO broadcast channels under limited feedback," *IEEE Trans. Inf. Theory*, vol. 58, no. 7, pp. 4509–4537, Jul. 2012.

[50] J. Hoydis, S. ten Brink, and M. Debbah, "Massive MIMO in the UL/DL of cellular networks: How many antennas do we need?" *IEEE J. Sel. Areas Commun.*, vol. 31, no. 2, pp. 160–171, Feb. 2013.

[51] E. Agrell, T. Eriksson, A. Vardy, and K. Zeger, "Closest point search in lattices," *IEEE Trans. Inf. Theory*, vol. 48, no. 8, pp. 2201–2214, Aug. 2002.

[52] U. Fincke and M. Pohst, "Improved methods for calculating vectors of short length in a lattice, including a complexity analysis," *Math. Comput.*, vol. 44, no. 170, pp. 463–471, Apr. 1985.

[53] S. Verdú, "Computational complexity of multiuser detection," *Algorithmica*, vol. 4, no. 1, pp. 303–312, 1989.

[54] Z.-Q. Luo, W.-K. Ma, A. M.-C. So, Y. Ye, and S. Zhang, "Semidefinite relaxation of quadratic optimization problems," *IEEE Signal Process. Mag.*, vol. 27, no. 3, pp. 20–34, May 2010.

[55] P. H. Tan and L. Rasmussen, "The application of semidefinite programming for detection in CDMA," *IEEE J. Sel. Areas Commun.*, vol. 19, no. 8, pp. 1442–1449, Aug. 2001.

[56] M. Bengtsson and B. Ottersten, "Optimal downlink beamforming using semidefinite optimization," in *Allerton Conf. Commun., Contr., Comput.*, Monticello, IL, Sep. 1999.

[57] N. D. Sidiropoulos, T. N. Davidson, and Z.-Q. Luo, "Transmit beamforming for physical-layer multicasting," *IEEE Trans. Signal Process.*, vol. 54, no. 6, pp. 2239–2251, Jun. 2006.

[58] S. Boyd and L. Vandenberghe, *Convex Optimization*. New York, NY, USA: Cambridge Univ. Press, 2004.

[59] O. Castañeda, T. Goldstein, and C. Studer, "Data detection in large multi-antenna wireless systems via approximate semidefinite relaxation," Sep. 2016. [Online]. Available: https://arxiv.org/abs/1609.01797

[60] N. Parikh and S. Boyd, *Proximal algorithms*. Now Publishers, 2013.

[61] T. Goldstein, C. Studer, and R. Baraniuk, "A field guide to forward-backward splitting with a FASTA implementation," Feb. 2016. [Online]. Available: https://arxiv.org/abs/1411.3406

[62] P. L. Lions and B. Mercier, "Splitting algorithms for the sum of two nonlinear operators," *SIAM J. Numer. Anal.*, vol. 16, no. 6, pp. 964–979, Dec. 1979.

[63] J. Eckstein and D. P. Bertsekas, "On the Douglas-Rachford splitting method and the proximal point algorithm for maximal monotone operators," *Math. Programming*, vol. 55, pp. 293–318, Apr. 1992.

[64] C. Studer and H. Bölcskei, "Soft-input soft-output single tree-search sphere decoding," *IEEE Trans. Inf. Theory*, vol. 56, no. 10, pp. 4827–4842, Oct. 2010.

[65] J. Jaldén and B. Ottersten, "On the complexity of sphere decoding in digital communications," *IEEE Trans. Signal Process.*, vol. 53, no. 4, pp. 1474–1484, Apr. 2005.

[66] D. Seethaler, J. Jaldén, C. Studer, and H. Bölcskei, "On the complexity distribution of sphere decoding," *IEEE Trans. Inf. Theory*, vol. 57, no. 9, pp. 5754–5768, Sep. 2011.

[67] S. Jacobsson, G. Durisi, M. Coldrey, U. Gustavsson, and C. Studer, "Throughput analysis of massive MIMO uplink with low-resolution ADCs," Jul. 2016. [Online]. Available: https://arxiv.org/abs/1602.01139